ACS OMEGA

Open Access

This article is licensed under CC-BY-NC-ND 4.0

http://pubs.acs.org/journal/acsodf

Article

Dual Activation of Peroxymonosulfate Using $MnFe_2O_4$/g-C_3N_4 and Visible Light for the Efficient Degradation of Steroid Hormones: Performance, Mechanisms, and Environmental Impacts

Kitipong Poomipuen, Chainarong Sakulthaew,* Chanat Chokejaroenrat, Athaphon Angkaew, Kanidrawee Techauay, Thapanee Poompoung, Kanokwan Teingtham, Piyaporn Phansak, Piyangkun Lueangjaroenkit, and Daniel D. Snow

Cite This: *ACS Omega* 2023, 8, 36136−36151

Read Online

ACCESS | Metrics & More | Article Recommendations | Supporting Information

ABSTRACT: Single activation of peroxymonosulfate (PMS) in a homogeneous system is sometimes insufficient for producing reactive oxygen species (ROS) for water treatment applications. In this work, manganese spinel ferrite and graphitic carbon nitride ($MnFe_2O_4$/g-C_3N_4; MnF) were successfully used as an activator for PMS under visible light irradiation to remove the four-most-detected-hormone-contaminated water under different environmental conditions. The incorporation of g-C_3N_4 in the nanocomposites led to material enhancements, including increased crystallinity, reduced particle agglomeration, amplified magnetism, improved recyclability, and increased active surface area, thereby facilitating the PMS activation and electron transfer processes. The dominant active radical species included singlet oxygen ($^1O_2$) and superoxide anions ($O_2^{\bullet-}$), which were more susceptible to the estrogen molecular structure than testosterone due to the higher electron-rich moieties. The self-scavenging effect occurred at high PMS concentrations, whereas elevated constituent ion concentrations can be both inhibitors and promoters due to the generation of secondary radicals. The MnF/PMS/vis system degradation byproducts and possible pathways of 17β-estradiol and 17α-methyltestosterone were identified. The impact of hormone-treated water on *Oryza sativa* L. seed germination, shoot length, and root length was found to be lower than that of untreated water. However, the viability of both ELT3 and Sertoli TM4 cells was affected only at higher water compositions. Our results confirmed that MnF and visible light could be potential PMS activators due to their superior degradation performance and ability to produce safer treated water.

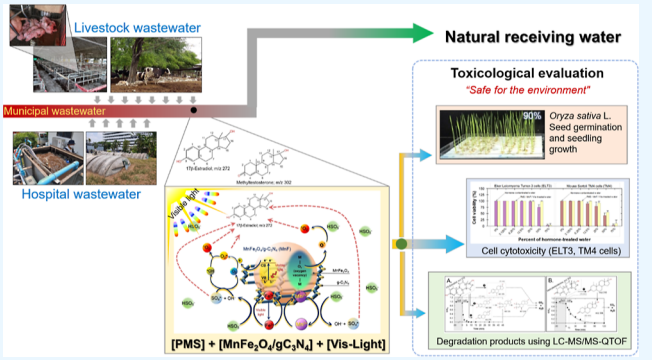

1. INTRODUCTION

The term "emerging contaminants" pertains to substances that have not yet undergone official regulatory measures or may be inadequately regulated. Examples of these compounds include pharmaceuticals (such as antibiotics and analgesics), pesticides (such as herbicides and insect repellents), industrial substances (such as disinfectants, nanomaterials, and microplastics), and endocrine disruptors (such as natural and synthetic hormones). Among these substances, steroid hormones have been identified as a significant and enduring hazard to both the environment and human health.[1] Upon repeated exposure to these compounds, even at very low concentrations (<1 ng L^{-1}), both the parent compounds and their metabolites have been observed to cause chronic toxicity.[2] Because several steroid hormones (e.g., 17β-estradiol, estradiol benzoate, and progesterone) have been authorized for use in food and animal production by the Food and Drug Administration (FDA) as a means of improving animal growth and increasing their annual productivity, these hormones are normally released from animal feedlots, animal feeding operations, and the dairy livestock industry.[3,4] Consequently, the presence of these hormones in natural receiving water is not an uncommon occurrence.

Endogenous hormones, 17β-estradiol (E2), the metabolite hormones, estrone (E1) and estriol (E3), and the androgenic hormone, 17α-methyltestosterone (MT), are usually found in subsurface water systems at very low concentrations due to their hydrophobicity and high adsorption capacity.[5] Their properties supported that sewage effluent, animal excrement,

Received: June 18, 2023
Accepted: August 31, 2023
Published: September 20, 2023

© 2023 The Authors. Published by American Chemical Society

and river sediment can be potential sinks for hormones.[6] On the contrary, the detection of hormone trace concentrations in natural water was widely reported in ng L^{-1}.[7] This was because hormones can display a more pronounced desorption effect at low concentrations, particularly when chemisorption is the dominant mechanism.[8] Moreover, Hildebrand et al.[9] also reported that finer-textured soils have a higher level of hormone desorption, which serves as a possible source of hormone release in water. Unfortunately, biodegradation and conventional chemical wastewater treatment methods cannot effectively eliminate the hormone, resulting in a trace amount of hormone remaining to be released into water as well.[10]

As a result, it has recently been shown that freshwater animals and the human body may carry some degree of hormone imbalance.[11] This long-term exposure likely increases the probability of human reproductive system cancer, weakens the immune system, and triggers cardiovascular diseases, as well as reducing of sperm count, vitellogenin production, and animal biomass in aquatic life.[11,12] The situation necessitates an effective methodology and robust treatment activity that are sufficient in addressing the issue of hormone-contaminated effluent water, which is imperative in preventing long-term exposure of both humans and aquatic life to contaminant residuals.

Persulfate-based advanced oxidation processes have been recognized as an effective method for treating wastewater due to their ability to produce active radicals. Peroxymonosulfate (HSO_5^-; PMS) and peroxydisulfate ($S_2O_8^{2-}$; PDS) have been favored over hydrogen peroxide (H_2O_2) due to their ability to produce a more superior sulfate radical ($SO_4^{\bullet-}$) than hydroxyl radical ($^{\bullet}OH$) upon activation. The energy transfer-based activation of PDS was proven to be efficacious and was relatively more suitable for PDS than PMS, but the single activation source (e.g., photo or heat activation) may be insufficient to produce an adequate amount of radicals.[13,14]

Given the aforementioned discussion, it is still debatable whether PMS or PDS is superior in being activated and generating $SO_4^{\bullet-}$. From a molecular structure standpoint, PDS exhibits a lower O−O bond dissociation energy compared to PMS, indicating that the O−O bond of PMS is more challenging to break.[15] Nevertheless, the PMS asymmetrical structure made PMS activation more effective than PDS, which possess a symmetrical structure.[16] While the generation of reactive oxygen species (ROS) from PDS activation is limited mostly to $SO_4^{\bullet-}$ and $^{\bullet}OH$, ROS generated from PMS activation can also include singlet oxygen ($^1O_2$) and the reaction is highly pH-dependent.[17] Numerous studies also confirmed that when using a heterogeneous activation system, PMS outperformed PDS in oxidizing organics through mediated electron transfer mechanisms and was also beneficial for material recycling.[18]

Using manganese ferrite ($MnFe_2O_4$) as a dual activator with visible light confers several advantages, including magnetic recyclability, excellent structural stability, efficient operation across a broad pH range (4−10), and the ability to absorb visible light (∼2.0 eV), which can occur synergistically during PMS activation.[19] Although cobalt ferrite ($CoFe_2O_4$) and $MnFe_2O_4$ have been competing with one another for activating PMS, $MnFe_2O_4$ has prevailed because Mn^{2+} is more environmentally friendly and naturally abundant.[20] Mn^{2+} and Fe^{2+} have been observed to provide a synergistic effect, enhancing the electron transfer efficiency and leading to increased production of ROS.[21] Because of its strong magnetism, $MnFe_2O_4$ tends to agglomerate, which reduces the number of active sites, which is a crucial factor for generating ROS.[22]

To enhance the practicality of $MnFe_2O_4$ for wastewater treatments, it is possible to employ graphitic carbon nitride (g-C_3N_4), a polymeric nonmetal semiconductor and promising two-dimensional photocatalyst, the synthesis process.[23] The g-C_3N_4 can help stabilize the morphological configuration of $MnFe_2O_4$ and can also function as a coordinating agent during the synthesis process.[24] In contrast, the activation of PMS using a semiconductor alone, such as g-C_3N_4, and graphene, was found to be insufficiently effective;[25] thus, it is necessary to include the doping material into the synthesis.

In this study, we synthesized $MnFe_2O_4$/g-C_3N_4 (MnF) to activate PMS and effectively degrade hormone-contaminated water. Four steroid hormones (E1, E2, E3, and MT) were investigated both collectively and separately. The objectives of this study were to (1) determine the hormone degradation efficiency using such an approach under different influential effects and (2) investigate the technical feasibility of using this newly developed treatment prior to releasing treated water into the natural receiving water. The effects of treated water on *Oryza sativa* L. seedling development and the cytotoxicity of ELT3 and TM4 cells were examined. E2 and MT degradation pathways are also proposed.

2. MATERIALS AND METHODS

Additional information containing additional materials and methods can be accessed in the Supporting Information. This includes information on the details of the chemicals (Section S1), material characterization (e.g., TEM, XRD, FTIR, and XPS) (Section S2), steroid hormone analyses (Section S3), and preparation of ELT3 and TM4 cell cultures (Section S4).

2.1. Material Synthesis. The MnF were synthesized using coprecipitation and melamine calcination methods, which were modified from Angkaew et al.[22] In brief, 0.2 M $MnSO_4{\cdot}H_2O$ (250 mL) and 0.4 M $FeCl_3{\cdot}6H_2O$ (250 mL) were mixed with 500 mL of DI water (80 °C, 1 h). Then, heated 8 M NaOH (80 °C) was slowly added for 1 h. Once pH 10.5 was reached, we stirred and maintained the solution for another hour. The solution was filtrated using a no. 4 Whatman filter paper. The precipitate was thoroughly washed with DI water several times to ensure a neutral pH followed by two cycles of ethanol washing and drying at 95 °C (2 h). Then, the obtained powder was ground with melamine at a ratio of 2:1 and calcined at 550 °C for 3 h, which was equivalent to 2:0.5 ($MnFe_2O_4$/g-C_3N_4).

2.2. Oxidative Enhancement Experiments. The catalytic activities of $MnFe_2O_4$/g-C_3N_4 (MnF) were evaluated by the removal of steroid hormones under different reaction conditions: (1) varying types of oxidizing agents (e.g., H_2O_2, PS, and PMS) without visible light irradiation; (2) with visible light irradiation. Tests were conducted with a 75 W halogen lamp illuminating the water surface perpendicularly. Unless otherwise specified, stock solutions (i.e., E1, E2, E3, and MT) were prepared in acetonitrile at concentrations of 100, 400, 400, and 200 mg L^{-1} and diluted with DI water to concentrations of 0.5, 2, 2, and 1 mg L^{-1} of E1, E2, E3, and MT, respectively (C_o). To reach equilibrium between adsorption and desorption on the MnF surface, 20 mg of the catalyst was dispersed in 100 mL of working solution and agitated in the dark for 30 min prior to the addition of the oxidant and the application of visible light. Each experimental unit was injected with 1 mL of PMS, PS, and 30% H_2O_2 to a final concentration of 300 mg L^{-1}. In the effects of the oxidant

https://doi.org/10.1021/acsomega.3c04333
ACS Omega 2023, 8, 36136−36151

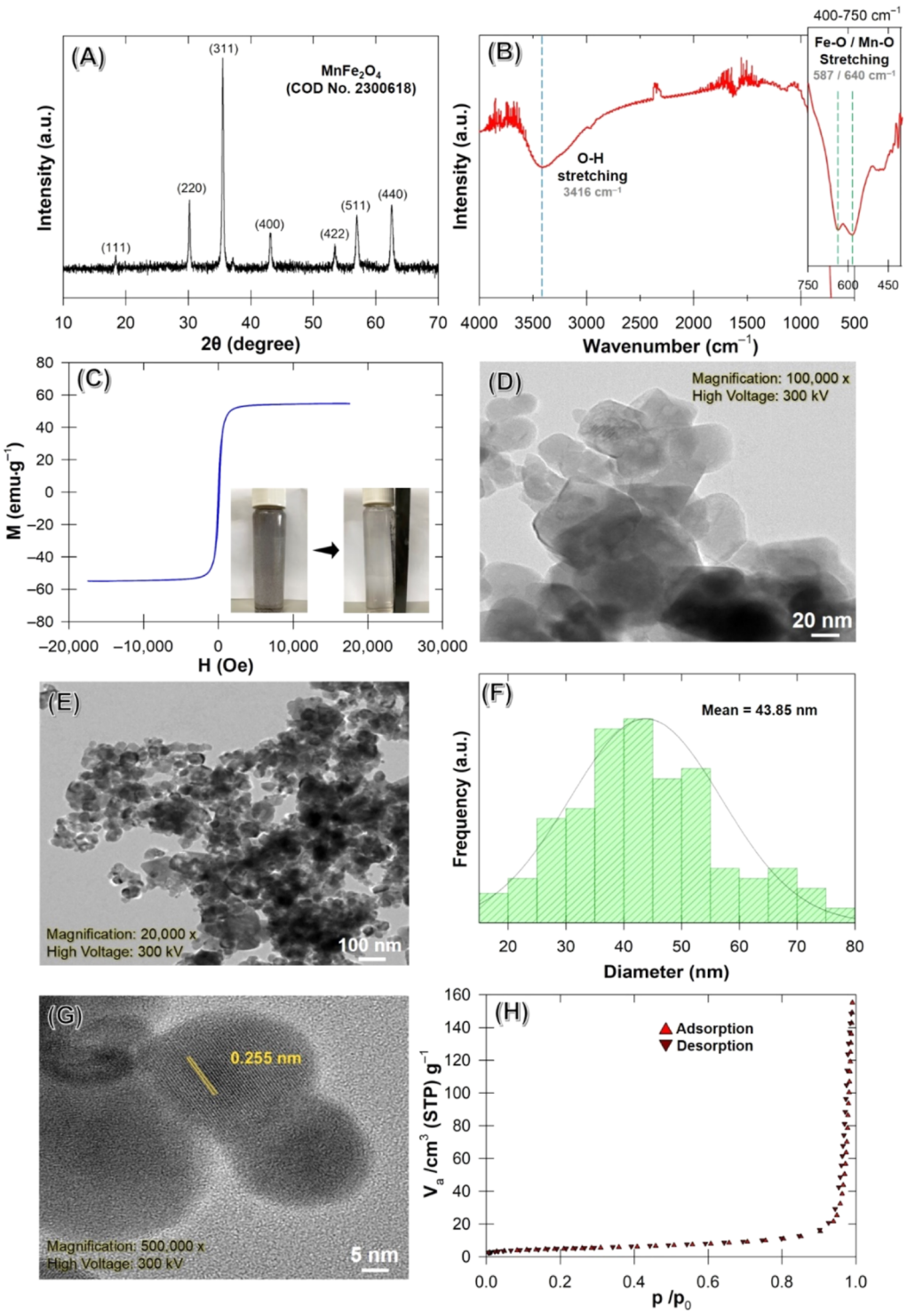

Figure 1. $MnFe_2O_4$/g-C_3N_4 nanoparticle (MnF) characteristics: (A) XRD spectra, (B) FTIR spectra, (C) VSM, (D,E) TEM images (magnification: 20,000×−100,000×), (F) particle size distribution, (G) HRTEM image (magnification: 500,000×), and (H) N_2 adsorption−desorption isotherm.

concentration experiment, each oxidant concentration was varied and the same protocol was followed. At each sampling period, 1 mL of the sample was quenched with 0.3 mL of ethanol to stop the reaction, filtered with a 0.45 m PTFE membrane filter, and transferred to a vial for HPLC analysis.

2.3. Scavenging Experiments at Varying pH. By introduction of a radical scavenger into each experimental unit, competition studies were undertaken to determine the dominant radical species in the process at each pH level. Tertbutyl alcohol (TBA; 117 mM), ethyl alcohol (EtOH; 117 mM), dimethyl sulfoxide (DMSO; 117 mM), furfuryl alcohol (FFa; 23.46 mM), and *p*-benzoquinone (*p*-BQ; 23.46 mM) were utilized to preferentially quench $^{\bullet}OH$, $SO_4^{\bullet-}$, electron (e^-), $^1O_2$, and $O_2^{\bullet-}$. The chemical probes were used individually: each of which served as a particular probe for one active radical while being considerably inert to others. In a

https://doi.org/10.1021/acsomega.3c04333
ACS Omega 2023, 8, 36136−36151

way, the most effective scavenger for that particular reactive oxidation species (ROS) on the hormone removal efficiency (i.e., least % removal) represents the dominant species for the reaction.

2.4. Influential Effects. The ion species and organic constituents that may be encountered in actual discharge water include pH (3−11), NO_3^- (1−40 mg L^{-1}), HCO_3^- (10−400 mg L^{-1}), Cl^- (10−1000 mg L^{-1}), and humic acid (50−150 mg L^{-1}), and we systematically manipulated the concentrations of these ions to their most possible detected levels. Experiments were conducted using PMS-activated MnF irradiated with visible light (PMS/MnF/vis) using the methodology described earlier, while each effect was independently varied. The initial concentration of the four steroid hormones examined ranged from 0.5 to 2 mg L^{-1}. In order to prevent interference with the PMS/MnF/vis reaction, no buffer was utilized throughout the experiment. Because actual discharge water is often associated with naturally existing other constituents, including a high load of organic matter, we selected real discharge water from a densely populated residential neighborhood in the Chatujak district, Bangkok, Thailand, where poultry farms are also located.

The determination of the point of zero charge (pH_{pzc}) was conducted because the pH could be interfered with by both the ionic species in solution and the MnF nanoparticle surface. Using either HCl (0.1 M) or NaOH (0.1 M) to adjust the pH, each 50 mL sodium chloride solution (0.01 M) was pH-adjusted to a designated pH (2 to 12). The MnF (0.12 g) was introduced into each container and subjected to continuous agitation for 48 h. The intersection of the pH-changing curve from the MnF-added solution and the initially measured pH curve is the MnF pH_{pzc}.

2.5. Toxicity Evaluation. *2.5.1. Rice Seed Germination.* The impact of treated water on seed germination and seedling growth was studied using rice (*O. sativa* L.) seeds cv. RD31 (a nonphotosensitive rice developed by the Rice Department of Thailand). In brief, we planted *O. sativa* L. seeds on paper that had been moistened with DI water (i.e., control) and with PMS-contaminated water and PMS-treated water at three different concentrations (30, 60, and 90%). The seven treatments were arranged in a completely randomized design (CRD), with four replications containing 100 seeds per replicate. Standard germination tests were performed using the ISTA protocol. Fifty seeds were planted on top of the three-layer paper placed inside a plastic box (19 cm × 28 cm × 11 cm), moistened with 60 mL of the tested solution, and incubated at room temperature (25 °C). After 14 days, the following measurements were used to assess the seed vigor and physiological performance: (1) shoot length (cm) measured from the ground level to the longest leaf's tip; (2) root length (cm) measured from the base of the stem to the tip of the longest root; and (3) seedling dry weight (mg $plant^{-1}$) measured after drying the seedlings in a hot air oven at 80 °C for 24 h. Averages were taken from evaluations of 10 randomly selected seedlings per replicate. Treatment means were compared using Tukey's Honest Significant Difference (HSD) at the 0.05 probability level ($p \leq 0.05$).

2.5.2. Cell Culture/Cytotoxicity. To determine the toxicity of steroid hormone intermediates, we employed Eker leiomyoma tumor-3 (ELT3) and mouse Sertoli TM4 cells as target cells. Because steroid hormones in polluted water can function as endocrine disruptors and interfere with reproductive hormones, we conducted an in vitro bioassay using the ATCC-purchased Eker leiomyoma tumor-3/ELT-3 uterine leiomyoma tumor cell line and the mouse Sertoli TM4 cell line (Manassas, VA, USA). To verify that no cytotoxicity was caused in these cells, PMS/MnF/vis-treated water with varied concentrations of DI water was tested for cell viability. We used two factors to evaluate the cell viability: (1) the optical density of each sample, which was determined using a microplate reader (Bio-Rad, Hercules, CA, USA), and (2) the visual observation of changes in the cell overall characteristics.

3. RESULTS AND DISCUSSION

3.1. Material Characterization. The catalyst diffractogram showed prominent peaks for the planes (111), (220), (311), (400), (422), (511), and (440) at 2θ values of 18.06, 29.71, 34.99, 42.52, 52.76, 56.20, and 61.69°, respectively, which correspond with the crystal planes of the $MnFe_2O_4$ spinel structure (COD no. 2300618) (Figure 1A). The catalyst crystallite size calculated from the (311) diffraction peak using Debye−Scherrer's equation was found to be 30.4 nm. The XRD result revealed that the catalyst was a high-crystalline spinel ferrite without impurities. By this synthesis method, the calcination of coprecipitate particles without the addition of melamine results in the formation of hematite (α-Fe_2O_3) impurity, which significantly decreases the magnetic saturation value (M_s), resulting in poor recoverability of the prepared catalyst.[24,27] This was also confirmed by the FTIR spectra that showed huge adsorption peaks in 400−700 cm^{-1} region, which can be attributed to the metal−oxygen bonds (Fe−O, Mn−O) occupied at the tetrahedral and octahedral sites of the spinel structure.[26] Both XRD and FTIR results confirmed our successfully synthesized catalyst using coprecipitation followed by the melamine-assisted calcination method. Angkaew et al.[27] reported that g-C_3N_4 served as a coordinating agent by forming a metal−melamine complex and/or conjugating with a metal oxide. Under the calcining temperature (550 °C), this complex can further decompose into a spinel ferrite structure and volatile gases (i.e., CO_X, NO_X, and NH_3), successfully preventing α-Fe_2O_3 formation. The coupling was one of the most effective methods for promoting charge separation in g-C_3N_4, thereby achieving significantly increased photocatalytic activities.[28] A comparison of synthesized material using a coprecipitation technique from other research studies is tabulated in Section S5 in the Supporting Information.

Typically, g-C_3N_4 has an intense diffraction peak at 27.93° (002), which corresponds to the interplanar stacking of a conjugated aromatic system with a *d*-space value of 0.319 nm.[29] On the contrary, no g-C_3N_4 peaks were identified in both XRD (i.e., at 2θ = 27.4°) and FTIR spectra (i.e., C−N), presumably due to the low melamine content during synthesis and the high ferrite dispersion that obscured g-C_3N_4 features (Figure 1A,B). This absence is not uncommon when using a low g-C_3N_4 composition as compared to the other main components.[22] The deposition of $MnFe_2O_4$ onto the g-C_3N_4 nanosheet has been demonstrated to induce modifications in the crystalline structure and polycondensation of the g-C_3N_4, resulting in enhanced performance.[30]

Because the catalyst magnetic properties play an important role in the determination of the catalyst reusability potential, we measured the magnitude of the *M*−*H* hysteresis loop of the freshly prepared catalyst. Results showed a saturation magnetization (M_s) of 54.89 emu g^{-1}, remnant magnetization (M_r) of 8.034 emu g^{-1}, and a coercive field (H_c) of 67.75 O_e, indicating

https://doi.org/10.1021/acsomega.3c04333
ACS Omega 2023, 8, 36136−36151

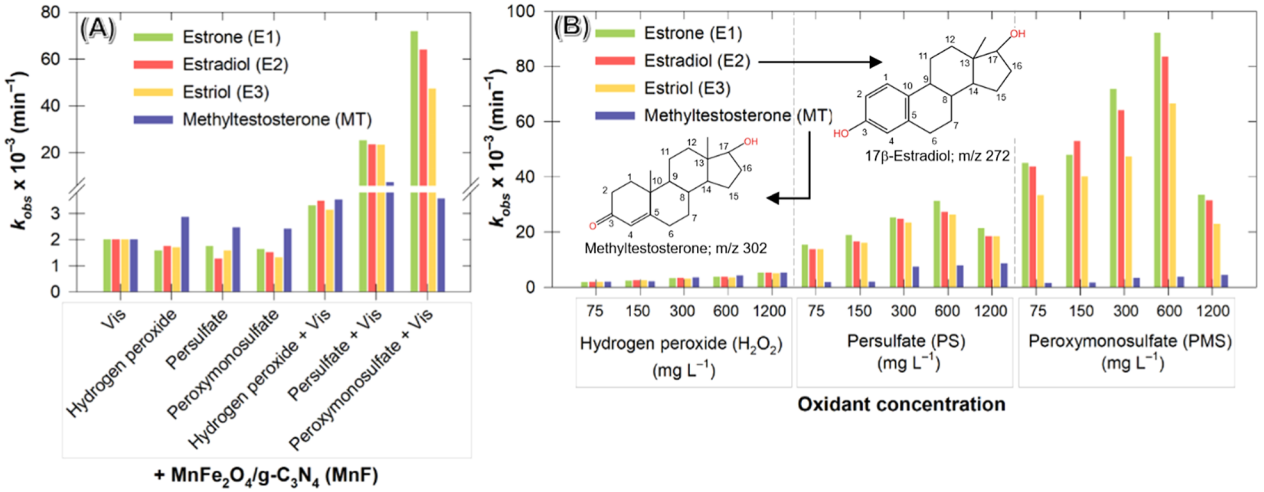

Figure 2. Pseudo-first-order degradation rate constant (k_{obs}) comparison of mix hormones following the treatment of different oxidative conditions with the $MnFe_2O_4$/g-C_3N_4 nanoparticle (MnF): (A) photocatalytic and/or oxidative activity and (B) varying oxidant dose (75−1200 mg L^{-1}).

a moderately high potential for recycling (Figure 1C). Furthermore, within a few minutes of placing an external magnet against the walls of the vial containing the catalyst solution, the solution turned crystal clear almost instantly, suggesting that our synthesis approach yields rapid recoverability and is appropriate for large-scale use. This was attributable to the addition of melamine during calcination, which resulted in stacking effects and increased the crystallinity of nanoparticles.

TEM images showed that both cubic and spherical structures ranging in size from 10 to 80 nm appeared in the prepared catalyst (Figure 1D,E). As compared to the calculated crystallite sizes (30.4 nm), the average particle size calculated by using ImageJ, which is an image processing application, was slightly higher (43.85 nm) (Figure 1F). The HR-TEM image of the catalyst showed lattice fringes of 0.255 nm corresponding to (311) that confirmed the nanoparticles of $MnFe_2O_4$ (Figure 1G). The adsorption−desorption isotherm illustrated the type-III isotherm with a small hysteresis loop with a mean pore diameter of 55.837 nm, implying that it was a typical macroporous material (Figure 1H).[31]

By modifying the Angkaew et al.[22] synthesis approach to be more practical for large-scale production by changing the chemical addition order and not dispersing material in methanol with sonication during the synthesis, the BET surface area increased by 1.2 folds (16.823 vs 7.04 m^2 g^{-1}) and a slight change in total pore volume (0.2348 $cm^2 \cdot g^{-1}$) was observed. This was done to avoid the potential issue of $MnFe_2O_4$ particles covering the g-C_3N_4 material and instead promote the embedding of $MnFe_2O_4$ particles onto the g-C_3N_4 surface, partially occupying its pores. However, these morphological characteristics validated its ideal activator for PMS, as a greater surface area can support both the electron transfer area and activating sites for active radical generation.

3.2. Oxidative Enhancement Experiments. Using a mixture of four steroid hormones as the sole carbon source under our experimental conditions, we showed a comparison of each hormone degradation rate (k_{obs}) under various oxidative systems (Figure 2A). The control test revealed negligible adsorption (<5%) occurred within the first 30 min. Without using the oxidant, no temporal changes in steroid hormones were observed, indicating that the photocatalytic reaction alone was insufficient to break down hormone molecules. This can be explained by the low performance of ROS generation (e.g., $E_{O_2^{\bullet -}}^{\circ}$ = +0.93 V) and the fact that MnF has lower valence band edge potentials and weak photoelectric conversion performance.

The $k_{obs\text{-}estrogens}$ were slower than $k_{obs\text{-}MT}$ by 5−10% when the oxidant was catalyzed by MnF without visible light, implying that the MT molecules were more susceptible to attack by $SO_4^{\bullet -}$ or $^{\bullet}OH$ than estrogens (Figure 2A). Although other reactive oxygen species (ROS) were present, the generated amount of radical species may have overshadowed other nonradical species and directly attacked the MT molecules. By including visible light in the reactions, the overall k_{obs} values were faster. This could be attributed to the oxidation capacity of photogenerated electrons−holes.

Although the $k_{obs\text{-}estrogen}$ following MnF/H_2O_2/vis treatment was >40% faster than without visible light, it was much less reactive as compared to the MnF/PS/vis and MnF/PMS/vis systems, indicating that PS or PMS activation occurred through transition metals in the MnF surface and subsequently generated more reactive species. The observed enhancement is indicative of a noteworthy synergistic outcome resulting from the combined utilization of photocatalysis and PMS oxidation processes. The catalytic activity was ranked in the order PMS > PS > H_2O_2, confirming that the generated $SO_4^{\bullet -}$ and $^{\bullet}OH$ were not the only reactive radicals in the system and that other ROS were more susceptible to the estrogens than those of $^{\bullet}OH$, thereby tremendously increasing $k_{obs\text{-}estrogens}$.

The increase in k_{obs} was due to the synergistic effect between photocatalysis and PS/PMS oxidation. This magnitude effect can be presented as the synergistic index (SI; $[k_{Ph+Pox}]/[k_{Ph} + k_{Pox}]$) using a formula modified from Chen et al.[32] where k_{Ph+Pox} is the k_{obs} obtained from the dual action of photocatalysis and the PS/PMS oxidation process, k_{Ph} is the k_{obs} obtained from photocatalysis alone, and k_{Pox} is the k_{obs} obtained from the PS/PMS oxidation process alone. By using $k_{obs\text{-}E2}$ as a target indicator obtained from the PS or PMS systems, the Supporting Information increased significantly from 7.0 to 19.39, respectively, indicating that the synergistic effect was predominant in the MnF activating process and that PMS oxidation was much more robust than PS oxidation.

Because the hormone degradation from the MnF/PMS/vis system was the most distinct, it can be further concluded that

https://doi.org/10.1021/acsomega.3c04333
ACS Omega 2023, 8, 36136−36151

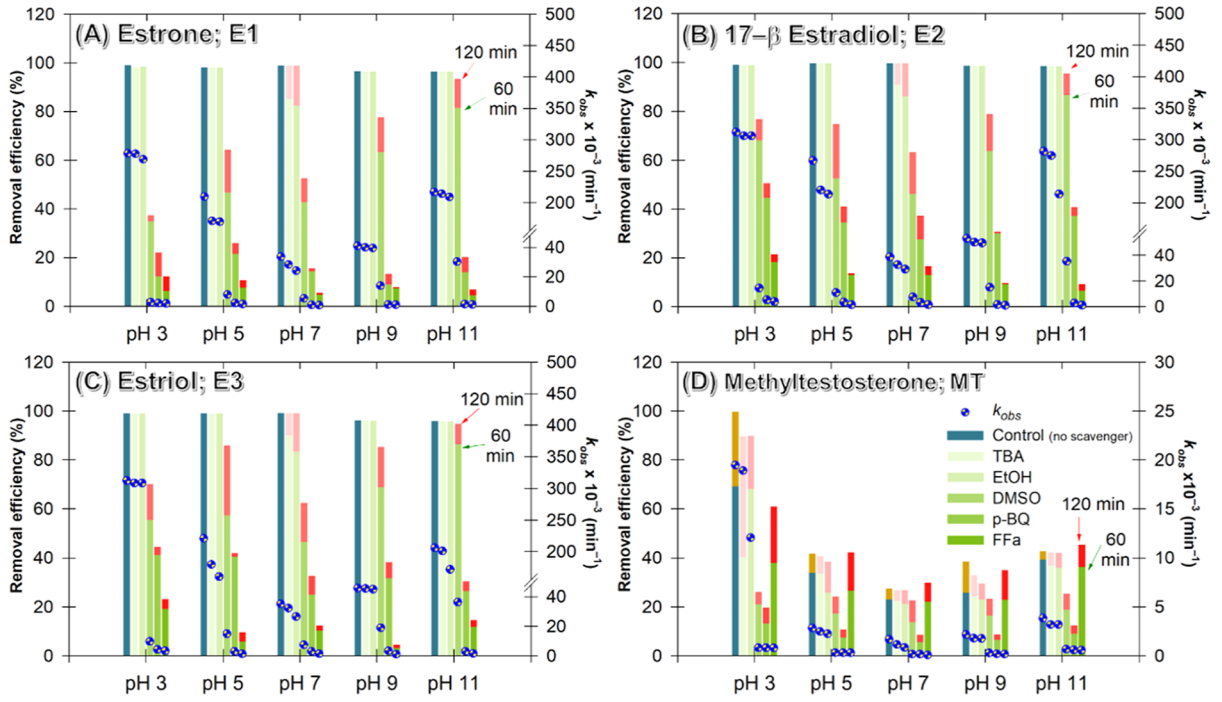

Figure 3. Hormone removal efficiencies [(A) estrone; (B) 17β-estradiol; (C) estriol; and (D) methyltestosterone] following treatment of the MnF/PMS/vis system at 60 and 120 min with the presence of radical scavengers (i.e., *tert*-butyl alcohol, TBA; ethanol, EtOH; dimethyl sulfoxide; DMSO; *para*-benzoquinone, *p*-BQ; and furfuryl alcohol, FFa) at varying pH (3−11). Pseudo-first-order degradation rate constants (k_{obs}) are shown using an additional *Y*-axis.

the hormone structure was prone to break down in the order of E1 > E2 > E3 > MT (e.g., $k_{obs\text{-}MT} = 3.5 \times 10^{-3}$ $min^{-1} \ll k_{obs\text{-}E2} = 62 \times 10^{-3}$ min^{-1}). However, without visible light irradiation, the order of degradation was reversed (i.e., MT > E3 > E2 > E1). This could be explained by (1) the difference in molecular structures of estrogens and testosterone and (2) the preferential path for a nonradical attack.

With visible light, the MnF/oxidant/vis generated active species in the following sequence: $^1O_2 > O_2^{\bullet-} > SO_4^{\bullet-} > {}^\bullet OH$. Li et al.[33] reported that $^1O_2$ and $O_2^{\bullet-}$ tend to target regions with higher electron-rich moieties, specifically the C1 to C5 sites on the estrogen molecules. Hence, the presence of a benzene ring resulted in an accelerated degradation rate of estrogen. Without visible light, the dominant species were identified as $SO_4^{\bullet-}$ or ${}^\bullet OH$, depending on the oxidant used, which exhibits a tendency toward molecular attack at the site of preferred electron transfer (i.e., C4−C5).[34] Here, the MT molecular structure was comparatively more prominent than that of estrogen. Consequently, a more rapid deterioration of the MT was observed.

Our results provided a positive correlation between oxidant and hormone degradation rates as they tentatively increased with the ROS generation, especially in the PS and PMS systems. Therefore, we varied the oxidant initial concentration (75−1200 mg L^{-1}) and maintained a constant MnF amount at 0.2 g L^{-1} under visible light irradiation (Figure 2B). The H_2O_2 at variation amounts showed only slight changes in k_{obs} regardless of hormone types, confirming our previous conclusion that hormone structure was more prone to react with $SO_4^{\bullet-}$ and other ROS than the ${}^\bullet OH$, and that MT molecular structure was similarly sensitive to the ${}^\bullet OH$ as compared to the estrogens. Both the MnF/PMS/vis and MnF/PS/vis systems also showed that the increase in oxidant concentrations increased the degradation rates (Figure 2B). The exception was at PS or PMS concentrations higher than 600 mg L^{-1}. The k_{obs} decreased by ∼40% for PS, while the k_{obs} decreased by ∼75% for PMS. The excess amount of PMS may potentially undergo a reaction with the produced $SO_4^{\bullet-}$ and ${}^\bullet OH$, leading to the formation of PMS radical ($SO_5^{\bullet-}$) and a self-scavenging effect.[35] Another plausible explanation is that the PMS structure exhibited a higher degree of dissociation compared to the PS structure, thereby accelerating a greater chance of this scavenging effect than PS does. Due to the apparent synergistic effects and high degradation rate, we opted to utilize 0.2 g L^{-1} MnF and 300 mg L^{-1} PMS for all subsequent experiments.

By using the spectrophotometric determination of PMS following the treatment of E2 under this condition, we found that the PMS concentration only decreased by 14.5%, which was consistent with other findings (see Section S6 in the Supporting Information). Given that E2 was degraded within 10 min of reaction and that real-world applications could use a higher PMS concentration to overcome the available organic constituents, the PMS amount can be considered sufficient for treating hormone-contaminated water. Further investigations were carried out to validate the inhibitory mechanism of O_2 in the solution (see Section S7 in the Supporting Information). The decrease in the dissolved oxygen (DO) concentration led to a reduction in the rate of degradation. This phenomenon may be attributed to the suppression of oxygen (O_2) which hinders the transfer of electrons from the valence band to the conduction band from the photocatalytic reaction. Consequently, the reaction is solely driven by the activation of PMS by MnF, without the involvement of electron transfer initiated from visible light.

3.3. Scavenging Experiments at Varying pH. By introducing various scavengers, we compared the differences in removal efficiencies at 60 and 120 min along with the k_{obs},

https://doi.org/10.1021/acsomega.3c04333
ACS Omega 2023, 8, 36136−36151

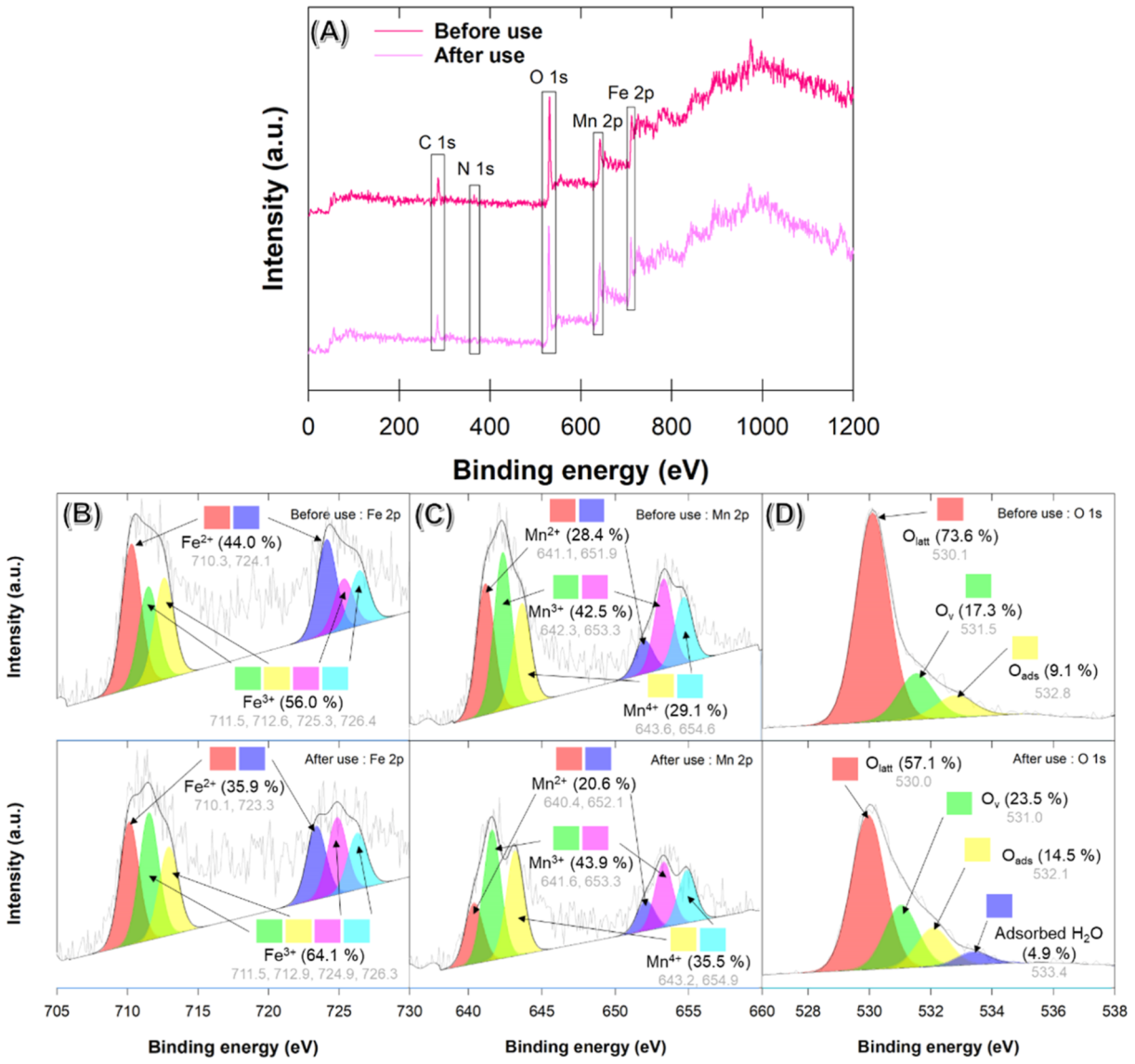

Figure 4. Changes in elemental composition of $MnFe_2O_4$/g-C_3N_4 nanoparticles (MnF) before and after activation: (A) XPS survey scan, (B) Fe 2s, (C) Mn 2s, and (D) O 1s XPS spectra.

which were determined from the beginning of the experiment to when the concentration remained less than 10%. In the control, all four hormones degraded in a similar manner at differing pH levels. Up to 95% of estrogens decreased within 60 min, while MT removal efficiencies were much slower, resulting in a 5- to 9-fold reduction in degradation rates. This can be explained by the preferential attack of the dominant active species, as discussed earlier.

In all tested pH ranges (3−11), the removal rates followed the order FFa > pBQ > DMSO > EtOH ≈ TBA as compared to the control (Figure 3). The scavenging experiment was done under visible light irradiation and without visible light irradiation (Section S8 in the Supporting Information). The degradation rate barely changed after the addition of TBA and EtOH, suggesting that $SO_4^{\bullet-}$ and $^{\bullet}OH$ were not the primary active species in the reaction. Meanwhile, both removal rates and degradation rates dropped dramatically once FFa and pBQ were introduced, demonstrating that $^1O_2$ and $O_2^{\bullet-}$ were the primary ROS involved, especially within the alkali/PMS system. By using both $^1O_2$ scavengers (i.e., FFa and NaN_3), results were similar, confirming that both scavengers can be used interchangeably (Section S8). Past research also showed that $^1O_2$ was more prominent in degrading contaminants, even though there were other reactive species associated with the PMS activation process.[36] It is noteworthy that MT exhibited the highest level of degradation at pH = 3, which is consistent with other observations that $SO_4^{\bullet-}$ and $^{\bullet}OH$ are the most effective under acidic conditions. Furthermore, it can be seen that the photogenerated e^- also plays a minor role in the degradation process as DMSO addition slightly affects the removal rates, indicating that there was some energy excitation generated following visible light irradiation (Figure 3).

3.4. Proposed Activation Mechanism. To find out what happens to the surface metal ions when PMS is activated by visible light and to prove that g-C_3N_4 exists, XPS spectra of both the new and used MnF nanocomposite were recorded. From the survey scan XPS spectra (Figure 4A), signals of C 1s, N 1s, O 1s, Mn 2p, and Fe 2p were detected in all samples at binding energy peaks of 285.0, 530.0, 641.0, and 711.0 eV, respectively.

https://doi.org/10.1021/acsomega.3c04333
ACS Omega 2023, 8, 36136−36151

Binding energy peaks at ∼711.5, ∼712.5 eV (Fe $2p_{3/2}$), and ∼725.3−726.4 eV (Fe $2p_{1/2}$) corresponded to Fe^{3+}, and the deconvoluted peaks of ∼710.3 and ∼724.1 eV were ascribed to Fe^{2+}. After activation with PMS under visible light irradiation, the Fe^{2+} content decreased (44.0 to 35.9%), while the Fe^{3+} content increased (56.0 to 64.1%), signifying the oxidation of Fe^{2+} to Fe^{3+} that also yielded the $SO_4^{\bullet-}$ (Table 1 and Figure 4B) [eq 1].[37]

Mn 2p XPS spectra showed two main peaks at binding energies ∼641.5 and ∼653.2 eV, which corresponded to Mn $2p_{3/2}$ and Mn $2p_{1/2}$. Mn $2p_{3/2}$ spectra revealed three deconvoluted peaks at 641.1, 642.3, and 643.6, which were ascribed to Mn^{2+}, Mn^{3+}, and n^{4+}, respectively.[38] After the reaction, the Mn^{2+} relative content decreased (28.4 to 20.6%), while Mn^{3+} slightly decreased (42.6 to 43.6%), and Mn^{4+} also increased (29.1 to 35.5%) (Figure 4C). These changes in Mn^{3+}/Mn^{4+} inferred that the activation with PMS also occurred on the catalyst surface to also generate the $SO_4^{\bullet-}$ [eq 2].[38]

During the PMS activation with the catalyst, the OH^- can simultaneously react with the available $SO_4^{\bullet-}$ to form $^{\bullet}OH$ molecules and oxygen [eq 3].[37] During the reaction, we also witnessed tiny bubbles in the solution, which could be confirmed as the result of the self-reaction between $SO_4^{\bullet-}$ and OH^-. Because we found that photogenerated e^- was slightly responsible for the reaction, we believe that the O_2 generation was part of our $O_2^{\bullet-}$ production [eqs 4 and 5]. Then, the available $^{\bullet}OH$ can further react with the recent form of $O_2^{\bullet-}$ to produce $^1O_2$ [eq 6].[22] Also, Guo et al.[39] reported that the O_2 can be from the reaction between Fe^{3+} and the $O_2^{\bullet-}$ that were available in the solution, we are skeptical that this reaction would occur under our experimental setup [eq 7]. If it was there, it might have been a rapid reaction, and the Fe^{3+} was insufficient to react with a large amount of $O_2^{\bullet-}$, thereby O_2 formation was only minimal. Moreover, Angkaew et al.[27] showed that the ferrites also have photocatalytic performance and were able to produce $^{\bullet}OH$ under light irradiation [eq 8]. Because of the $O_2^{\bullet-}$ abundance, we ruled out that, once released, the $^{\bullet}OH$ would simultaneously react and provide more $^1O_2$ into the system, concordant with our scavenging experiment that rooted for $^1O_2$ production.

The O 1s spectra showed four peaks at binding energies of ∼530.0, ∼531.5, ∼532.8, and ∼533.4 eV (Figure 4D), which were attributed to the lattice oxygen (O_{latt}) (i.e., Fe−O, Mn−O), the oxygen vacancy (O_V), the adsorbed oxygen (O_{ads}), and adsorbed H_2O, respectively.[22,40,41] The adsorbed H_2O was also confirmed by the FTIR fingerprint (i.e., OH stretching at 3416 cm^{-1}) (Figure 1B). An obvious decrease in O_{latt} (73.6 to 57.1%) with an increase in O_V (17.3 to 23.5%) was observed, indicating the release of O_{latt}, possibly to maintain the electric neutrality of transformed metal ions [eq 9].[38,42] Increases in the level of O_{ads} (9.1 to 14.5%) and adsorbed H_2O (4.9%) may have resulted from the O_V adsorbing some oxygen-containing molecules such as O_2, hydroxyl-like groups, and H_2O. The decrease in the level of O_{latt} after the activation indicated that some O_{latt} could be transformed to active oxygen (O*) [eq 10]. As the scavenging experiment established that $^1O_2$ was the most prominent (ROS) in the PMS activation, we inferred that it originated from this O* generation that can consequently react with PMS (HSO_5^-) to yield $^1O_2$ [eq 11].[39]

It was evidenced that MnF activated with the available PMS in the solution with visible light, resulting from the continual activation from the regeneration of metal ions on the MnF surface. When surrounded by PMS, these oxidized metals [i.e., Fe^{3+} and $Mn^{(n+1)+}$] could react and form a PMS radical

Table 1. Chemical Equations in the Dual Activation of Peroxymonosulfate Using $MnFe_2O_4$/g-C_3N_4 Nanoparticles (MnF) and Visible Light Irradiation under Varying Treatment Conditions[a]

reactions	Eqs
$Fe^{2+} + HSO_5^- \rightarrow Fe^{3+} + SO_4^{\bullet-} + OH^-$ (1)	1
$Mn^{n+} + HSO_5^- \rightarrow Mn^{(n+1)+} + SO_4^{\bullet-} + OH^-$ (2)	2
$2SO_4^{\bullet-} + 2OH^- \rightarrow 2SO_4^{2-} + 2^{\bullet}OH + O_2$ (3)	3
$MnF + h_v \rightarrow e^- + h^+$ (4)	4
$O_2 + e^- \rightarrow O_2^{\bullet-}$ (5)	5
$O_2^{\bullet-} + {}^{\bullet}OH \rightarrow {}^1O_2 + OH^-$ (6)	6
$Fe^{3+} + O_2^{\bullet-} \rightarrow Fe^{2+} + O_2$ (7)	7
$Fe^{3+} + h_v + H_2O \rightarrow Fe^{2+} + {}^{\bullet}OH + H^+$ (8)	8
$M^{3+}–O^{2-}–M^{3+} \rightarrow M^{3+}–O_V–M^{3+} + O^*$ (9)	9
$O_{latt} \rightarrow O^*$ (10)	10
$O^* + HSO_5^- \rightarrow HSO_4^- + {}^1O_2$ (11)	11
$Fe^{3+} + HSO_5^- \rightarrow Fe^{2+} + SO_5^{\bullet-} + H^+$ (12)	12
$Mn^{(n+1)+} + HSO_5^- \rightarrow Mn^{n+} + SO_5^{\bullet-} + H^+$ (13)	13
$Mn^{3+} + Fe^{2+} \rightarrow Mn^{2+} + Fe^{3+}$ (14)	14
$HSO_5^- \rightarrow SO_5^{2-} + H^+$ (15)	15
$SO_4^{\bullet-} + OH^- \rightarrow SO_4^{2-} + {}^{\bullet}OH$ (16)	16
$^{\bullet}OH + OH^- \rightarrow O^{\bullet-} + H_2O$ (17)	17
$HSO_5^- + H_2O \rightarrow HSO_4^- + H_2O_2$ (18)	18
$SO_5^{2-} + H_2O \rightarrow SO_4^{2-} + H_2O_2$ (19)	19
$HSO_5^- + SO_5^{2-} \rightarrow HSO_4^- + SO_4^{2-} + {}^1O_2$ (20)	20
$H_2O_2 \rightarrow 2^{\bullet}OH$ (21)	21
$^{\bullet}OH + H_2O_2 \rightarrow {}^{\bullet}OOH + H_2O$ (22)	22
$^{\bullet}OOH \rightarrow O_2^{\bullet-} + H^+$ (23)	23
$^{\bullet}OOH + {}^{\bullet}OOH \rightarrow {}^1O_2 + H_2O_2$ (24)	24
$2O_2^{\bullet-} + 2H^+ \rightarrow {}^1O_2 + H_2O_2$ (25)	25
$NO_3^- + h_v \rightarrow NO_2^{\bullet} + O^{\bullet-}$ (26)	26
$NO_3^- + SO_4^{\bullet-} \rightarrow NO_3^{\bullet} + SO_4^{2-}$ (27)	27
$NO_3^- + {}^{\bullet}OH \rightarrow NO_3^{\bullet} + OH^-$ (28)	28
$HCO_3^- + SO_4^{\bullet-} \rightarrow CO_3^{\bullet-} + SO_4^{2-} + H^+$ (29)	29
$HCO_3^- + SO_4^{\bullet-} \rightarrow HCO_3^{\bullet-} + SO_4^{2-}$ (30)	30
$HCO_3^- + {}^{\bullet}OH \rightarrow CO_3^{\bullet-} + H_2O$ (31)	31
$Cl^- + SO_4^{\bullet-} \leftrightarrow Cl^{\bullet} + SO_4^{2-}$ (32)	32
$Cl^- + {}^{\bullet}OH \leftrightarrow Cl^{\bullet} + OH^-$ (33)	33
$HSO_5^- + Cl^- \rightarrow SO_4^{2-} + HOCl$ (34)	34
$Cl^{\bullet} + H_2O \rightarrow HOCl^{\bullet-} + H^+$ (35)	35
$HSO_5^- + 2Cl^- + H^+ \rightarrow SO_4^{2-} + H_2O + Cl_2$ (36)	36
$HOCl^{\bullet-} \leftrightarrow Cl^- + {}^{\bullet}OH$ (37)	37

[a]References are given in the text.

https://doi.org/10.1021/acsomega.3c04333
ACS Omega 2023, 8, 36136−36151

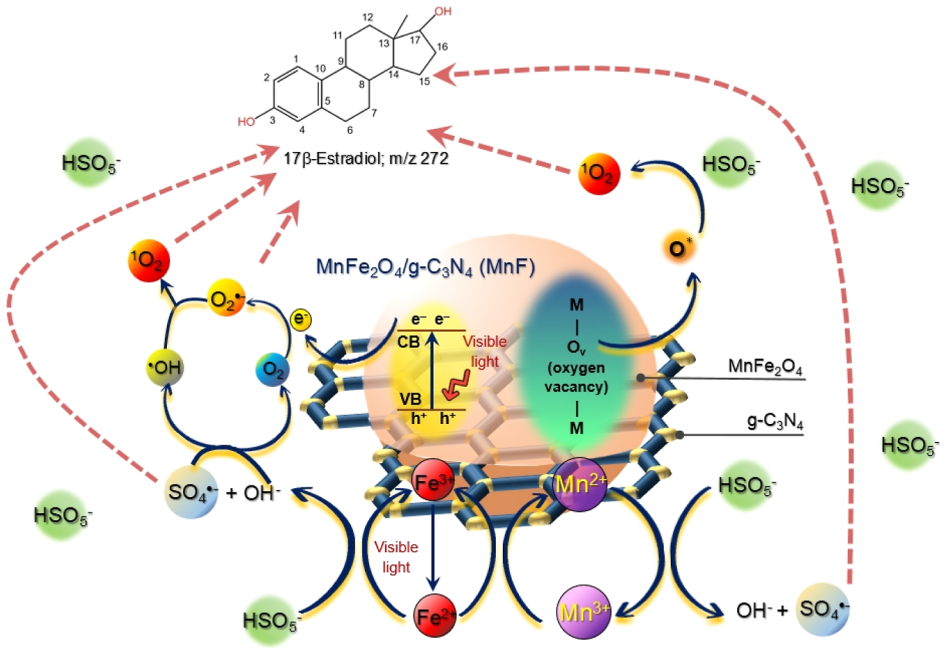

Figure 5. Proposed photocatalytic/activation mechanism for steroid hormone degradation following MnF/PMS under visible light irradiation.

Table 2. Comparison of the Observed Degradation Rate Constant (k_{obs}) at Different Influential Effects (i.e., pH, NO_3^-, HCO_3^-, Cl^-, Humic Acids, and Actual Wastewater)

varied parameter	value	$k_{obs} \times 10^{-3}$ (min^{-1}), (± % difference)			
		E1	E2	E3	MT
none	control	71.9 (0)	64.2 (0)	47.5 (0)	3.6 (0)
pH	3	312.4 (+334.6)	312.4 (+386.8)	278.6 (+486.9)	19.5 (+445.4)
	5	221 (+207.4)	267.2 (+316.3)	209.7 (+341.8)	2.8 (−20.4)
	7	35.1 (−51.2)	38.77 (−39.6)	33.69 (−29.0)	1.7 (−52.6)
	9	45.7 (−36.5)	53.12 (−17.2)	41.02 (−13.6)	2.2 (−39.2)
	11	206.1 (+186.7)	281.9 (+339.2)	217.1 (+357.3)	3.8 (+7.8)
NO_3^- ($mg \cdot L^{-1}$)	1	74.7 (+3.8)	67.4 (+5.0)	49.6 (+4.5)	3.5 (−3.2)
	2	78.7 (+9.5)	72.5 (+12.9)	54.2 (+14.1)	3.8 (+5.8)
	5	89.6 (+24.6)	81.8 (+27.5)	60.6 (+27.7)	3.9 (+8.0)
	10	99.6 (+38.6)	90.0 (+40.3)	66.8 (+40.6)	4.1 (+13.6)
	20	121.0 (+67.9)	111.1 (+73.1)	83.4 (+75.8)	4.2 (+16.4)
	40	112.6 (+56.6)	102.9 (+60.3)	76.0 (+60.0)	4.1 (+16.0)
HCO_3^- ($mg \cdot L^{-1}$)	10	8.0 (−88.9)	8.5 (−86.8)	9.4 (−80.2)	2.6 (−26.3)
	50	13.3 (−81.5)	14.0 (−78.2)	14.5 (−69.5)	2.7 (−24.3)
	100	16.5 (−77.0)	16.9 (−73.7)	16.6 (−65.1)	2.8 (−23.0)
	200	36.8 (−48.8)	34.1 (−46.9)	28.4 (−40.3)	3.1 (−13.6)
Cl^- ($mg \cdot L^{-1}$)	40	60.0 (−16.5)	53.4 (−16.8)	39.4 (−17.0)	2.9 (−17.5)
	100	35.7 (−50.4)	33.7 (−47.5)	27.5 (−42.0)	2.1 (−40.9)
	500	60.9 (−15.2)	54.6 (−14.9)	39.0 (−17.8)	3.0 (−14.7)
	1000	84.1 (+17.0)	75.0 (+16.9)	54.0 (+13.8)	4.5 (+25.7)
humic acid ($mg \cdot L^{-1}$)	50	56.7 (−21.1)	53.2 (−17.0)	34.7 (−26.9)	2.9 (−16.7)
	100	51.9 (−27.8)	51.7 (−19.4)	30.3 (−36.2)	2.8 (−22.5)
	150	46.2 (−35.8)	45.5 (−29.0)	27.1 (−42.8)	2.5 (−29.3)
wastewater		62.5 (−13.0)	33.3 (−48.1)	22.1 (−53.5)	1.4 (−60.2)

($SO_5^{\bullet -}$) [eqs 12 and 13].[38,39] Zhang et al.[43] reported that $SO_5^{\bullet -}$ could induce a mild reaction with organic contaminants due to its low 1.1 V redox potential. Moreover, the electron transfer between these Mn and Fe redox reactions can always favorably occur [eq 14], which improved electron transfer and redox cycling of metal ions, supported the continual input of these ions into the reaction system, and led to an increase in O_V.

Based on the above investigation, we proposed three main mechanisms involved in the continued loss of hormone concentration through $^1O_2$ production (Figure 5): (1) an activation causing electron transfer between metal ions and HSO_5^-; (2) the reaction between O* and HSO_5^-; and (3) the photogenerated e^-.

3.5. Influential Effect Experiments. Again, a mixture of hormones was used, and a temporal change of each hormone

https://doi.org/10.1021/acsomega.3c04333
ACS Omega 2023, 8, 36136−36151

was individually determined and reported as its degradation rate (Table 2). Overall, the degradation pattern of each hormone, was found to be consistent under previously conducted conditions (E1 > E2 > E3 ≫ MT), indicating that the system was set up consistently.

3.5.1. Effect of pH. Results showed that our oxidative system was suitable for treating hormones in a wide pH range (3−11) as compared to the control (∼pH 5.9). As can be seen, the increase in k_{obs} under an alkaline condition was excessively high for estrogens, but slightly higher than the control for MT (Table 2). This was attributed to the high pK_a of all three estrogens (pK_{aE1} = 10.77, pK_{aE2} = 10.71, and pK_{aE3} = 10.46).[44] Once the solution pH was beyond these pK_a, these uncharged estrogens underwent rapid transformation and potentially impeded chromatographic determination, thereby possibly overestimating degradation efficiency. MT, however, exhibited a significantly higher pK_a value of 15.4, rendering it considerably more stable across a wide range of pH values.[45] Consequently, we used MT to elucidate the correlation between elevated pH and hormone degradation.

Only a slight increase in k_{obs} was observed at an alkaline pH (+7.8%). Rani et al.[46] reported that PMS possessed a pK_a of 9.4, making it self-deprotonating to SO_5^- under an alkaline condition (Table 1) [eq 15].

The MnF pH_{zpc} was determined to be 6.6; therefore, the catalyst surface was negatively charged under this pH condition. Therefore, the electrostatic repulsion between PMS and MnF occurred under this pH condition, possibly decreasing the MT removal. Given this degradation impediment, MT decomposition was still revealed, which could be from the available reactive oxygen species in the aqueous solution that continually occur at a constant rate. Our earlier proposed activation mechanism revealed that $^1O_2$ was the major reactive species under similar conditions following the initial formation of $SO_4^{\bullet-}$ from the HSO_5^- activation with the MnF catalyst surface [eqs 1 and 2]. In the alkaline condition, hydroxide ions were reported to cause a scavenging effect on initially generated radicals (e.g., $SO_4^{\bullet-}$, $^\bullet$OH) [eqs 16 and 17].[47] Because the instant reactions between the available OH^- and these radicals were rapid,[48] the $O_2^{\bullet-}$ were also rapidly generated, which can continuously form $^1O_2$ and directly attack the MT molecules [eq 6].

Moreover, both HSO_5^- and SO_5^{2-} can be continually hydrolyzed, undergo chain reactions to produce $^1O_2$, and interconvert to form H_2O_2, which could further react with available $^\bullet$OH to form hydroperoxyl radicals ($^\bullet$OOH) [eqs 18−22].[49] Because of the $^\bullet$OOH instability, it can be both self-decomposed and self-reacted to generate both $O_2^{\bullet-}$ and $^1O_2$ [eqs 23−25].[50] Overall, the alkaline condition amplifies the formation of $^1O_2$, thereby increasing its reactivity and supplementing the degradation efficiency of MT. This finding validated our previously proposed mechanisms, which suggest that the oxidative system generates a steady supply of $^1O_2$ through both photocatalysis and PMS activation pathways.

3.5.2. Effects of Constituent Anions. Results showed that an increase in the NO_3^- concentration increased the hormone degradation rates (Table 2). Nitrate is ubiquitous in natural receiving water and was reported to cause a positive impact on the $SO_4^{\bullet-}$ oxidation at <20 mg L^{-1} and a negative impact on the $^\bullet$OH oxidation at <2 mg L^{-1}.[51,52]

In this study, visible light irradiation acted synergistically with the MnF activated PMS. It is highly plausible that the changes of NO_3^- to secondary radicals could be attributed to light irradiation. According to Keen et al.,[53] nitrate has the ability to react with visible light in water treatment systems, resulting in the formation of $^\bullet$OH through oxygen radicals ($O^{\bullet-}$) (Table 1) [eq 26]. The $O^{\bullet-}$ was then hydrolyzed to form $^\bullet$OH, which exhibited greater reactivity toward organic compounds.[53] As discussed earlier, $SO_4^{\bullet-}$ and $^\bullet$OH served as intermediate radicals to form $^1O_2$. These two radicals could also react with NO_3^-, which acted as a radical scavenger, to form a strong radical like $NO_3^\bullet$ (E° = 2.5 V) [eqs 27 and 28].[54] It is noted that the presence of NO_3^- had a beneficial effect on the generation of $SO_4^{\bullet-}$, regardless of whether the activation process was homogeneous (using PS/UV) or heterogeneous (using PMS/catalyst).[51]

Unlike that of NO_3^-, the probability of HCO_3^- undergoing reactions with visible light to generate other radicals is low. However, HCO_3^- was also found to scavenge both active radicals ($SO_4^{\bullet-}$ and $^\bullet$OH) and consequently form the carbonate radicals, which have a relatively high redox potential (E° = 1.78 V) [eqs 29−31].[55] As previously reported, bicarbonate and carbonate have been identified as both potential inhibitors and promoters even at minimal concentrations,[56] posing a challenge in determining their precise function within our oxidative system. In this study, with the existence of this alkalinity, the k_{obs} were initially retarded and continued to increase with an increase in HCO_3^- concentration (Table 2). Although other possible self-reactions of $CO_3^{\bullet-}$ are possible, the function of $CO_3^{\bullet-}$ in drinking water with its prominent radicals is not widely understood. Ji et al.[57] found that the impact of HCO_3^- on the oxidative system was negligible within the range of 0−610 mg L^{-1}. Considering that wastewater discharged from livestock farming typically exhibits alkalinity levels <55 mg L^{-1},[58] the presence of HCO_3^- may therefore not significantly impede degradation efficiency.

In contrast to the NO_3^-, the existence of Cl^- hindered the k_{obs}; however, a higher concentration of Cl^- may marginally enhance the k_{obs}, albeit it is still lower than the control. Numerous studies have revealed that Cl^- can also react with both radicals generated from PMS, resulting in the formation of chlorine radicals ($Cl^\bullet$) that exhibit lower reactivity [eqs 32−37].[51,55] Results indicated that a low concentration of Cl^- (<500 mg L^{-1}) can have a negative impact on the presence of the two active radicals and the formation of $^1O_2$, thereby impeding the oxidation of contaminants. Because $^1O_2$ cannot convert Cl into low reactivity reactive species (e.g., HOCl, Cl_2 and $Cl^\bullet$), a decrease in k_{obs} can be expected.[59]

Nevertheless, when the concentration of Cl^- surpasses 1000 mg L^{-1}, it is plausible for $Cl^\bullet$ to undergo direct oxidation, leading to the formation of $HOCl^{\bullet-}$ and $^\bullet$OH [eqs 35 and 37].[55] The formation of hypochlorous acid (HOCl) and dichlorine (Cl_2) is also a plausible outcome when excess chloride reacts with residual PMS, thereby enhancing degradation efficiency [eqs 34 and 36]. Similar observations at high Cl^- concentrations were reported for the treatment of E2 and triclosan.[26,51]

3.5.3. Effects of Natural Organic Matter. Since humic acids (HA) comprise a significant portion of natural organic matter (NOM), we varied the HA concentration up to 150 mg L^{-1}. Results demonstrated that the increase in HA progressively reduced the level of steroid hormone degradation (Table 2). The inhibition effect was caused by the competitive reaction between the steroid hormone and HA with reactive radicals and nonradical species. It is also possible that HA could be adsorbed onto the active sites of the material surface,

https://doi.org/10.1021/acsomega.3c04333
ACS Omega 2023, 8, 36136−36151

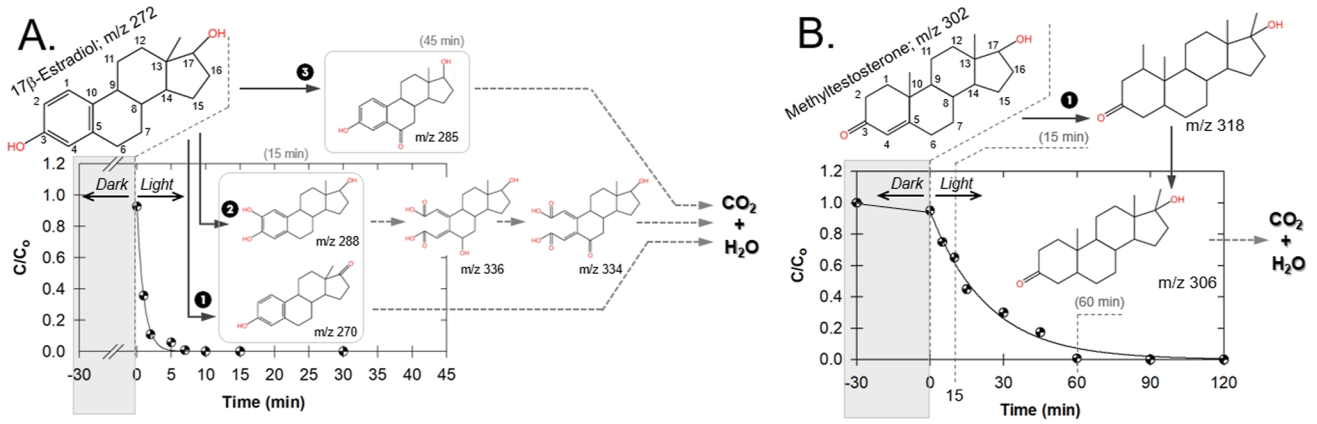

Figure 6. Proposed E2 (A) and MT (B) degradation pathways following MnF/PMS under visible light irradiation.

potentially reducing the activation efficiency of PMS.[60] Additionally, the HA exhibited comparable turbidity, which may obstruct the transmission of visible light and impede the initiation of activation for the generation of reactive species. This information revealed that our treatment would likely be more successful if a filtration system was implemented to facilitate the separation of humic colloids from the water.

To further evaluate the real discharge water, we collected wastewater from the poultry farm in Chatujak district, Bangkok, and used it as real water matrices. Results showed that the degradation efficiency decreased by 13−60.2% (Table 2). We believe that the high reduction in disparity was not solely attributable to the inhibitory impact, but rather to the high k_{oc} of hormones, with MT being the highest, followed by E3, E2, and E1.[5] The efficacy of steroid degradation is hindered primarily by the presence of suspended solids and NOM in the wastewater. Given that these hormones can be naturally adsorbed through organic colloids, several studies have demonstrated that hormones that are adsorbed onto particles can be released gradually and dissolved in the surrounding water. Therefore, strong and robust oxidative treatment is still necessary.

3.5.4. Stability and Reusability Test. Two primary concerns associated with the utilization of MnF for the remediation of contaminants are (1) the compatibility and reusability of this material in practical, real-world situations and (2) the potential negative environmental repercussions of these nanocomposites. The investigation of reusability was conducted through a series of four-cycle experiments (see Section S9 in the Supporting Information). Results showed that the degradation efficiencies observed in each cycle were relatively consistent (Section S9). However, the rate of degradation during the initial cycle was slightly higher compared with subsequent cycles. Most importantly, only slight leaching concentration of metals (Mn and Fe concentration) were observed following the treatment (Section S10). These experiments demonstrated the material's durability, as it remained functional for up to four cycles while effectively degrading hormone-contaminated water.

3.6. Proposed Degradation Products of MT and E2. Through the use of the LC−MS/MS-QTOF, the E2 degradation mechanism following the MnF/PMS/vis system was determined. After 30−45 min of E2 oxidation, three possible pathways were proposed: (1) via estrone or E1 (m/z 270), (2) via 2-hydroxy estradiol (m/z 288), and (3) via the ketone intermediate (m/z 285) (Figure 5A).

Pathway 1: the detection of E1 ($C_{18}H_{22}O_2$; m/z 270) after 30 min of reaction time suggests an alternative pathway involving the oxidation of the hydroxyl group of the E2 five-membered ring.[61] Pathway 2: the ROS is prone to attack at the C2 site to generate a hydroxyl group (2-hydroxy estradiol; m/z 288) and then further oxidize at C2 and C3 to produce carboxyl groups (Figure 6A).[61] Then, Hu et al.[62] reported that the C6 site of the E2 structure is susceptible to electro-electrical attack, which could result in the formation of a hydroxyl group at this carbon position to form $C_{18}H_{24}O_6$ (m/z 336).[61] The m/z 336 could undergo a dehydrogenation reaction to become a carbonyl group, forming $C_{18}H_{22}O_6$ (m/z 334). Despite the absence of these two compounds in our analysis, it is postulated that a direct route to mineralization is also possible.

Pathway 3: due to the high electron density at C6 of the aliphatic ring of E2,[63] the detection of the third possible degradation product ($C_{18}H_{21}O_3$, m/z 285; ketone intermediate) was detected at 45 min of the reaction. Further oxidation of these compounds with continual production of ROS within the system would also likely result in the formation of organic acids and then carbon dioxide and water. Therefore, the oxidative fate of these compounds under the reported conditions is likely to be complete mineralization.

The degradation mechanism of MT was determined through the utilization of GC/MS. As an MT complete removal was longer than that of E2, the MT treatment was conducted for 60 min so that the generated oxygen species would have sufficient time to reach all MT molecules. The mass spectra showed major intermediate molecular ion peaks of m/z 318 (15 min) and m/z 306 (60 min).

A possible mechanism for the MT degradation based on literature precedent revealed that it could be initiated by the hydrogen abstraction reaction, which is likely to occur at the C6 atom. This process may lead to the formation of an observed intermediate compound (m/z 318). Subsequently, m/z 318 may undergo further oxidation to yield m/z 306. Under our experimental conditions, achieving complete mineralization with minimal catalyst and oxidant dosage was unlikely without the assistance of biological treatment.[64] In addition, Fragkaki et al.[65] proposed that the initiation of MT breakdown may result in the formation of a more hydrophilic compound. This compound is expected to have weaker androgenic activity compared to MT.

3.7. Toxicity Evaluation. *3.7.1. O. sativa L. Seed Germination.* Results showed that the before treatment

https://doi.org/10.1021/acsomega.3c04333
ACS Omega 2023, 8, 36136−36151

(A)

Treatment	%	Germination (%)		Shoot length (cm)		Root length (%)		Seedling dry weight (g plant^{-1})	
DI water	0	100.00	a	9.73 ± 0.29	a	4.49 ± 0.62	a	0.088 ± 0.01	a
Before treatment	30	91.50 ± 5.00	b	7.19 ± 0.20	c	2.62 ± 0.19	c	0.070 ± 0.01	a
	60	97.50 ± 1.91	a	8.08 ± 1.28	b	3.21 ± 0.47	bc	0.070 ± 0.01	a
	90	85.00 ± 8.08	c	5.72 ± 0.25	d	2.41 ± 0.71	c	0.048 ± 0.02	b
After treatment	30	98.50 ± 1.91	a	8.95 ± 0.39	ab	3.98 ± 0.70	ab	0.080 ± 0.01	a
	60	99.50 ± 1.00	a	8.82 ± 0.22	b	3.14 ± 0.25	bc	0.085 ± 0.02	a
	90	99.50 ± 1.00	a	8.53 ± 0.56	b	2.90 ± 0.72	c	0.080 ± 0.01	a
CV (%)		3.91		7.09		17.28		16.22	

Remark: Pairwise Mean Comparison of Treatments using Tukey's Honest Significant Difference (HSD) at 0.05 (95%)

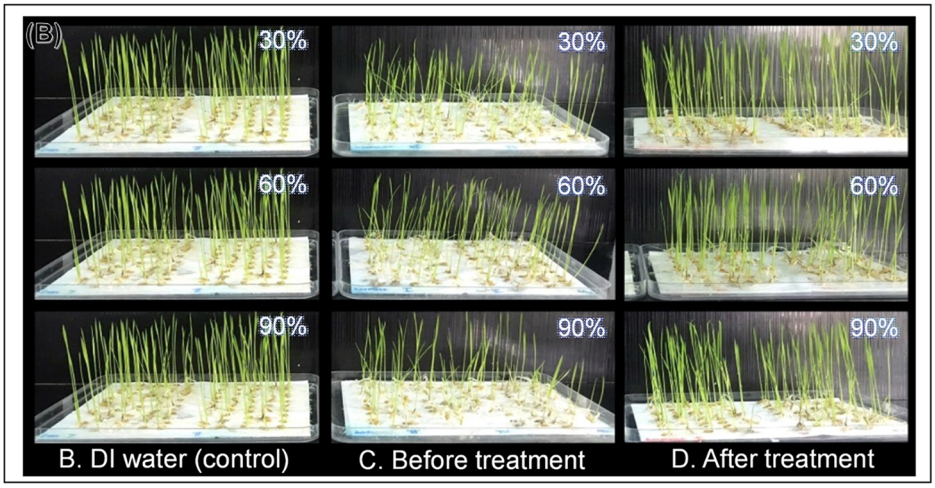

Figure 7. (A) Comparison of *O. sativa* L. seed germination and seedling growth characteristics after exposure to different compositions of DI water (i.e., control), hormone-contaminated water (i.e., before treatment), and hormone-treated water (i.e., after treatment). (B) Photograph of *O. sativa* L. seedling growth planted on paper moistened with different treatments.

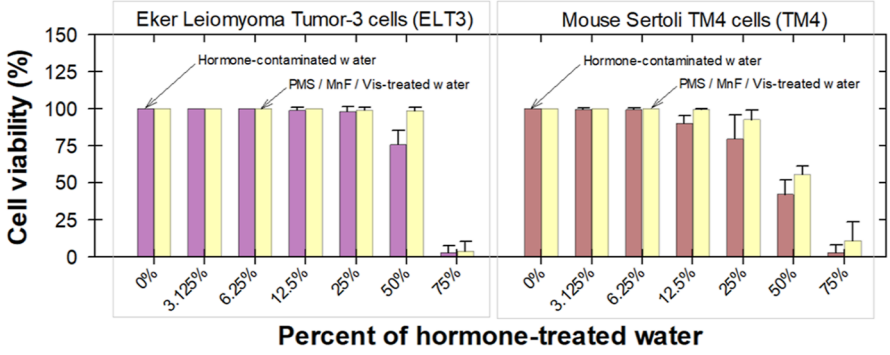

Figure 8. ELT3 and TM4 cell cytotoxicity after exposure to different compositions of hormone-contaminated water (i.e., before treatment) and hormone-treated water (i.e., after treatment).

water had a negative impact on germination, shoot length, and root length of *O. sativa* L. seeds, while the seedling dry weight only had a negative impact at the highest composition (i.e., 90%) (Figure 6A). The root length had the most significant negative effect, with a decrease of up to 46% compared to the control. The hormone concentration in planted water was found to be a controlling factor for the changes in oxidative stress during germination as it showed relatively varied results. Erdal and Dumlupinar[66] reported that a trace amount of E2 (10^{-6} to 10^{-10} M) increased α-amylase activity and the antioxidant enzyme activities for chickpea, thereby promoting seed germination and seedling growth. The E2 concentration of 1.83×10^{-6} to 10^{-8} M can also enhance the shoot and root dry weight of alfalfa (*Medicago sativa* L.), while at a concentration higher than 1.83×10^{-4} M, the plant growth starts to dwindle.[67] A similar observation was found for the reduction of seed germination and seedling growth of corn seeds (*Zea mays* L.) at a concentration of 3.6×10^{-5} M.[68]

Once exposed to the treated water, results revealed that there were no significant changes in germination or seedling dry weight. This indicated that active radicals may have already long dissipated and that SO_4^{2-} and hormone residuals are not sufficiently high to compromise seedling growth. Notably, the K^+ and Mn^{2+} residuals from the PMS from treated sulfathiazole water were found to stimulate wheat and radish growth planted in treated soil better than that of untreated soil.[69] On the contrary, the shoot length and root length of rice in our study were negatively impacted and decreased their length by 12.3

https://doi.org/10.1021/acsomega.3c04333
ACS Omega 2023, 8, 36136−36151

and 35.4%, respectively (Figure 7B). Xu et al.[70] also reported this similar finding in rice growth after exposure to unnaturally high anionic constituents. These results confirmed that the treated water still needed to be diluted prior to use for irrigation.

3.7.2. ELT3 and TM4 Cell Cytotoxicity. Following the effect of treated water on rice seed germination, the question pertaining to the safety of the treated water for other living organisms that exhibit a greater degree of hormonal responsiveness, such as reproductive organs, still remains. Consequently, Sertoli TM4 and ELT3 cells were utilized as representative target cells to receive mixed hormone-treated water at varying percentages. Results showed that, when exposed to 0−25% of hormone-treated water, none of the samples demonstrated significant cytotoxicity (i.e., >75% cell viability) (Figure 8). In addition, we found that the cytotoxicity potential started at ≥50% water composition for ELT3 and ≥12.5% water composition for TM4. The treated water was safer for the cells by a margin of 15−25%, indicating a slight negative impact from our treatment. This trend could be associated with the dissipation of reactive oxygen species (ROS) that have a relatively short lifespan and the fact that the hormone-degradates had less estrogenic activity toward the tested cells. Notably, the observed difference in viability was less prominent at 75% of the water composition, indicating that cellular sensitivity to hormones would be heightened, irrespective of treatment status. This result provided evidence that the treated water would need to be diluted before being released into the natural receiving water in order to prevent harm to any living cells.

Numerous studies have indicated that exposure to excess endocrine-disrupting chemicals (EDCs), such as exogenous androgen or estrogen, may have an impact on uterine fibroids and disrupt reproductive organs. This effect is believed to be due to the stimulation of the Fas apoptosis pathways or a direct effect on mitochondrial function through the downregulation of antiapoptotic members of the Bcl-2 family, resulting in cell apoptosis.[71] Since ELT3 and TM4 cells are similar and possess the Fas cell signaling pathway, they are susceptible to interference by foreign substances or these extraordinary high exogenous hormones.[72]

As can be seen, in our experimental conditions, TM4 was more responsive as it started to reveal its marginal effects at as low as 12.5% water composition. This could be associated with the high proportion of female hormone to male hormone, which was 1:4:3.7:1.8 (molar basis) for E1, E2, and MT, respectively. The ELT3 exhibited greater tolerance than TM4 when subjected to a 50% water composition. However, even ELT3 was unable to counteract the high levels of estrogenic activity resulting from a high dose of estrogen, particularly at a water composition exceeding 75%. We believe that one of the hormone degradates, which could be considered to have time- and dose-dependent effects, significantly suppressed the level of intratesticular testosterone, making TM4 less tolerable. Consequently, exposure to a high dose resulted in the stimulation of apoptosis and facilitated the occurrence of necrosis. It is recommended that a gradual discharge of treated water be implemented, and further research should be conducted to thoroughly examine the mechanisms of cellular degradation and the remnants of estrogenic activity in treated water.

4. CONCLUSIONS

The effectiveness of using manganese spinel ferrite and graphitic carbon nitride ($MnFe_2O_4$/g-C_3N_4; MnF) and visible light to activate PMS in removing steroid hormones from aqueous solutions has been demonstrated. The PMS/visible light oxidation processes were significantly improved by the newly developed MnF. The singlet oxygen ($^1O_2$) was found to be the dominant reactive oxygen species that was supported by the formation of superoxide anions ($O_2^{\bullet-}$), sulfate radicals ($SO_4^{\bullet-}$), hydroxyl radicals ($^\bullet$OH) and photogenerated e^-. Both 17β-estradiol (E2) and 17α-methyltestosterone (MT) degradation pathways following the MnF/PMS/vis system were investigated. The hormone-treated water was safer for *O. sativa* L. seed germination and seedling growth. However, it was only safe for ELT3 and Sertoli TM4 cells at water compositions <50 and <25%, respectively. The present investigation provided novel perspectives on wastewater treatment strategies through the use of MnF and visible light as activators for PMS oxidation to solve environmental issues.

■ ASSOCIATED CONTENT

Supporting Information

The Supporting Information is available free of charge at https://pubs.acs.org/doi/10.1021/acsomega.3c04333.

Details of the chemicals; material characterization; steroid hormone analyses; preparation of ELT3 and TM4 cell cultures; comparison for materials synthesized from the coprecipitation method; PMS residuals following the oxidative system; degradation efficiency under a O_2-deficiency condition; $^1O_2$ confirmation using different chemical probes; stability test of material following the oxidative treatment; and metal leaching concentration following treatment under different pH values (PDF)

■ AUTHOR INFORMATION

Corresponding Author

Chainarong Sakulthaew − *Department of Veterinary Technology, Faculty of Veterinary Technology, Kasetsart University, Bangkok 10900, Thailand; Department of Veterinary Nursing, Faculty of Veterinary Technology, Kasetsart University, Bangkok 10900, Thailand;* orcid.org/0000-0001-6489-1373; Phone: +66-2942-8900 ext. 616018; Email: cvtcns@ku.ac.th

Authors

Kitipong Poomipuen − *Department of Veterinary Technology, Faculty of Veterinary Technology, Kasetsart University, Bangkok 10900, Thailand*

Chanat Chokejaroenrat − *Department of Environmental Technology and Management, Faculty of Environment, Kasetsart University, Bangkok 10900, Thailand*

Athaphon Angkaew − *Department of Environmental Technology and Management, Faculty of Environment, Kasetsart University, Bangkok 10900, Thailand*

Kanidrawee Techauay − *Department of Veterinary Technology, Faculty of Veterinary Technology, Kasetsart University, Bangkok 10900, Thailand*

Thapanee Poompoung − *Department of Veterinary Technology, Faculty of Veterinary Technology, Kasetsart University, Bangkok 10900, Thailand*

https://doi.org/10.1021/acsomega.3c04333
ACS Omega 2023, 8, 36136−36151

Kanokwan Teingtham − *Department of Agronomy, Faculty of Agriculture at Kamphaeng Sean, Kasetsart University, Nakhon Pathom 73140, Thailand*

Piyaporn Phansak − *Division of Biology, Faculty of Science, Nakhon Phanom University, Nakhon Phanom 48000, Thailand*

Piyangkun Lueangjaroenkit − *Department of Microbiology, Faculty of Science, Kasetsart University, Bangkok 10900, Thailand*

Daniel D. Snow − *School of Natural Resources and Nebraska Water Center, Part of the Robert B. Daugherty Water for Food Global Institute, 202 Water Sciences Laboratory, University of Nebraska-Lincoln, Lincoln, Nebraska 68583-0844, United States;* orcid.org/0000-0003-0885-0504

Complete contact information is available at: https://pubs.acs.org/10.1021/acsomega.3c04333

Author Contributions

Conceptualization, C.S.; methodology, C.S. and K.P.; validation, C.S., C.C., and A.A.; formal analysis, C.S. and C.C.; investigation, K.P., K.T., T.P., K.T., and P.P.; resources, C.S.; data curation, C.S. and C.C.; writing—original draft preparation, C.S. and C.C.; writing—review and editing, C.S., C.C., K.P., P.L., and D.S.; visualization, C.S. and C.C.; supervision, C.S.; project administration, C.S.; and funding acquisition, C.S. All authors have read and agreed to the published version of the manuscript.

Notes

The authors declare no competing financial interest.

■ ACKNOWLEDGMENTS

This research was funded by Kasetsart University through the Graduate School Fellowship Program and the Office of the Ministry of Higher Education, Science, Research and Innovation and the Thailand Science Research and Innovation through the Kasetsart University Reinventing University Program 2021. The authors also gratefully acknowledge the Faculty of Environment and the Faculty of Veterinary Technology, Kasetsart University, for providing facility support and access to analytical instruments.

■ REFERENCES

(1) Xu, P.; Zhou, X.; Xu, D.; Xiang, Y.; Ling, W.; Chen, M. Contamination and Risk Assessment of Estrogens in Livestock Manure: A Case Study in Jiangsu Province, China. *Int. J. Environ. Res. Public Health* **2018**, *15* (1), 125.

(2) Gunnarsson, L.; Snape, J. R.; Verbruggen, B.; Owen, S. F.; Kristiansson, E.; Margiotta-Casaluci, L.; Österlund, T.; Hutchinson, K.; Leverett, D.; Marks, B.; et al. Pharmacology beyond the patient−The environmental risks of human drugs. *Environ. Int.* **2019**, *129*, 320−332.

(3) Aroeira, C. N.; Feddern, V.; Gressler, V.; Contreras-Castillo, C. J.; Hopkins, D. L. A review on growth promoters still allowed in cattle and pig production. *Livest. Sci.* **2021**, *247*, 104464.

(4) Food and Drug Administration Home Page. Steroid Hormone Implants Used for Growth in Food-Producing Animals. https://www.fda.gov/animalveterinary/safetyhealth/productsafetyinformation/ucm055436.htm (accessed June 04, 2023).

(5) Card, M. L.; Chin, Y.-P.; Lee, L. S.; Khan, B. Prediction and Experimental Evaluation of Soil Sorption by Natural Hormones and Hormone Mimics. *J. Agric. Food Chem.* **2012**, *60* (6), 1480−1487.

(6) Kostich, M.; Flick, R.; Martinson, J. Comparing predicted estrogen concentrations with measurements in US waters. *Environ. Pollut.* **2013**, *178*, 271−277.

(7) Goeury, K.; Munoz, G.; Vo Duy, S.; Prévost, M.; Sauvé, S. Occurrence and seasonal distribution of steroid hormones and bisphenol A in surface waters and suspended sediments of Quebec, Canada. *Environ. Adv.* **2022**, *8*, 100199.

(8) Durán-Álvarez, J. C.; Prado, B.; Ferroud, A.; Juayerk, N.; Jiménez-Cisneros, B. Sorption, desorption and displacement of ibuprofen, estrone, and 17β estradiol in wastewater irrigated and rainfed agricultural soils. *Sci. Total Environ.* **2014**, *473*−*474*, 189−198.

(9) Hildebrand, C.; Londry, K. L.; Farenhorst, A. Sorption and Desorption of Three Endocrine Disrupters in Soils. *J. Environ. Sci. Health, Part B* **2006**, *41* (6), 907−921.

(10) Hakk, H.; Sikora, L.; Casey, F. X. M. Fate of estrone in laboratory-scale constructed wetlands. *Ecol. Eng.* **2018**, *111*, 60−68.

(11) Moore, S. C.; Matthews, C. E.; Ou Shu, X.; Yu, K.; Gail, M. H.; Xu, X.; Ji, B.-T.; Chow, W.-H.; Cai, Q.; Li, H.; et al. Endogenous Estrogens, Estrogen Metabolites, and Breast Cancer Risk in Postmenopausal Chinese Women. *JNCI, J. Natl. Cancer Inst.* **2016**, *108* (10), djw103.

(12) Hallgren, P.; Nicolle, A.; Hansson, L.-A.; Brönmark, C.; Nikoleris, L.; Hyder, M.; Persson, A. Synthetic estrogen directly affects fish biomass and may indirectly disrupt aquatic food webs. *Environ. Toxicol. Chem.* **2014**, *33*, 930−936.

(13) Sakulthaew, C.; Chokejaroenrat, C.; Satapanajaru, T.; Chirasatienpon, T.; Angkaew, A. Removal of 17β-Estradiol Using Persulfate Synergistically Activated Using Heat and Ultraviolet Light. *Water, Air, Soil Pollut.* **2020**, *231* (5), 247.

(14) Shah, N. S.; He, X.; Khan, H. M.; Khan, J. A.; O'Shea, K. E.; Boccelli, D. L.; Dionysiou, D. D. Efficient removal of endosulfan from aqueous solution by UV-C/peroxides: A comparative study. *J. Hazard. Mater.* **2013**, *263*, 584−592.

(15) Benson, S. W. Thermochemistry and kinetics of sulfur-containing molecules and radicals. *Chem. Rev.* **1978**, *78* (1), 23−35.

(16) Gao, Y.; Zhu, Y.; Lyu, L.; Zeng, Q.; Xing, X.; Hu, C. Electronic Structure Modulation of Graphitic Carbon Nitride by Oxygen Doping for Enhanced Catalytic Degradation of Organic Pollutants through Peroxymonosulfate Activation. *Environ. Sci. Technol.* **2018**, *52* (24), 14371−14380.

(17) Neta, P.; Huie, R. E.; Ross, A. B. Rate Constants for Reactions of Inorganic Radicals in Aqueous Solution. *J. Phys. Chem. Ref. Data* **1988**, *17* (3), 1027−1284.

(18) Ahn, Y.-Y.; Yun, E.-T.; Seo, J.-W.; Lee, C.; Kim, S. H.; Kim, J.-H.; Lee, J. Activation of Peroxymonosulfate by Surface-Loaded Noble Metal Nanoparticles for Oxidative Degradation of Organic Compounds. *Environ. Sci. Technol.* **2016**, *50* (18), 10187−10197.

(19) He, F.; Lu, Z.; Song, M.; Liu, X.; Tang, H.; Huo, P.; Fan, W.; Dong, H.; Wu, X.; Han, S. Selective reduction of Cu2+ with simultaneous degradation of tetracycline by the dual channels ion imprinted POPD-CoFe2O4 heterojunction photocatalyst. *Chem. Eng. J.* **2019**, *360*, 750−761.

(20) Pradhan, P.; Giri, J.; Samanta, G.; Sarma, H. D.; Mishra, K. P.; Bellare, J.; Banerjee, R.; Bahadur, D. Comparative evaluation of heating ability and biocompatibility of different ferrite-based magnetic fluids for hyperthermia application. *J. Biomed. Mater. Res., Part B* **2007**, *81B* (1), 12−22.

(21) Zhang, M.; Gong, Y.; Ma, N.; Zhao, X. Promoted photoelectrocatalytic degradation of BPA with peroxymonosulfate on a MnFe2O4 modified carbon paper cathode. *Chem. Eng. J.* **2020**, *399*, 125088.

(22) Angkaew, A.; Chokejaroenrat, C.; Sakulthaew, C.; Mao, J.; Watcharatharapong, T.; Watcharenwong, A.; Imman, S.; Suriyachai, N.; Kreetachat, T. Two facile synthesis routes for magnetic recoverable MnFe2O4/g-C3N4 nanocomposites to enhance visible light photo-Fenton activity for methylene blue degradation. *J. Environ. Chem. Eng.* **2021**, *9* (4), 105621.

(23) Cao, S.; Yu, J. g-C3N4-Based Photocatalysts for Hydrogen Generation. *J. Phys. Chem. Lett.* **2014**, *5* (12), 2101−2107.

(24) Yang, L.; Zhang, Y.; Liu, X.; Jiang, X.; Zhang, Z.; Zhang, T.; Zhang, L. The investigation of synergistic and competitive interaction

between dye Congo red and methyl blue on magnetic MnFe2O4. *Chem. Eng. J.* **2014**, *246*, 88−96.
(25) Yao, Y.; Lian, C.; Wu, G.; Hu, Y.; Wei, F.; Yu, M.; Wang, S. Synthesis of "sea urchin"-like carbon nanotubes/porous carbon superstructures derived from waste biomass for treatment of various contaminants. *Appl. Catal., B* **2017**, *219*, 563−571.
(26) Wang, Z.; Lai, C.; Qin, L.; Fu, Y.; He, J.; Huang, D.; Li, B.; Zhang, M.; Liu, S.; Li, L.; et al. ZIF-8-modified MnFe2O4 with high crystallinity and superior photo-Fenton catalytic activity by Zn-O-Fe structure for TC degradation. *Chem. Eng. J.* **2020**, *392*, 124851.
(27) Angkaew, A.; Sakulthaew, C.; Nimtim, M.; Imman, S.; Satapanajaru, T.; Suriyachai, N.; Kreetachat, T.; Comfort, S.; Chokejaroenrat, C. Enhanced Photo-Fenton Activity Using Magnetic Cu0.5Mn0.5Fe2O4 Nanoparticles as a Recoverable Catalyst for Degrading Organic Contaminants. *Water* **2022**, *14* (22), 3717.
(28) Chen, J.; Zhao, D.; Diao, Z.; Wang, M.; Shen, S. Ferrites boosting photocatalytic hydrogen evolution over graphitic carbon nitride: a case study of (Co, Ni)Fe2O4 modification. *Sci. Bull.* **2016**, *61* (4), 292−301.
(29) Xing, W.; Li, C.; Chen, G.; Han, Z.; Zhou, Y.; Hu, Y.; Meng, Q. Incorporating a novel metal-free interlayer into g-C3N4 framework for efficiency enhanced photocatalytic H2 evolution activity. *Appl. Catal., B* **2017**, *203*, 65−71.
(30) Palanivel, B.; Mudisoodum perumal, S. d.; Maiyalagan, T.; Jayarman, V.; Ayyappan, C.; Alagiri, M. Rational design of ZnFe2O4/g-C3N4 nanocomposite for enhanced photo-Fenton reaction and supercapacitor performance. *Appl. Surf. Sci.* **2019**, *498*, 143807.
(31) Burhan, M.; Shahzad, M. W.; Ng, K. C. Energy distribution function based universal adsorption isotherm model for all types of isotherm. *Int. J. Low-Carbon Technol.* **2018**, *13* (3), 292−297.
(32) Chen, X.; Zhou, J.; Chen, Y.; Zhou, Y.; Ding, L.; Liang, H.; Li, X. Degradation of tetracycline hydrochloride by coupling of photocatalysis and peroxymonosulfate oxidation processes using CuO-BiVO4 heterogeneous catalyst. *Process Saf. Environ. Prot.* **2021**, *145*, 364−377.
(33) Li, Z.; Sun, Y.; Liu, D.; Yi, M.; Chang, F.; Li, H.; Du, Y. A Review of Sulfate Radical-Based and Singlet Oxygen-Based Advanced Oxidation Technologies: Recent Advances and Prospects. *Catalysts* **2022**, *12* (10), 1092.
(34) Mahdi Ahmed, M.; Barbati, S.; Doumenq, P.; Chiron, S. Sulfate radical anion oxidation of diclofenac and sulfamethoxazole for water decontamination. *Chem. Eng. J.* **2012**, *197*, 440−447.
(35) Liu, Y.; Guo, H.; Zhang, Y.; Cheng, X.; Zhou, P.; Deng, J.; Wang, J.; Li, W. Highly efficient removal of trimethoprim based on peroxymonosulfate activation by carbonized resin with Co doping: Performance, mechanism and degradation pathway. *Chem. Eng. J.* **2019**, *356*, 717−726.
(36) Tien, Y. C.; Li, B.; Zhang, T.; Scott, A.; Murray, R.; Sabourin, L.; Marti, R.; Topp, E. Impact of dairy manure pre-application treatment on manure composition, soil dynamics of antibiotic resistance genes, and abundance of antibiotic-resistance genes on vegetables at harvest. *Sci. Total Environ.* **2017**, *581*−*582*, 32−39.
(37) Zhou, R.; Liu, S.; He, F.; Ren, H.; Han, Z. Alkylpolyglycoside modified MnFe2O4 with abundant oxygen vacancies boosting singlet oxygen dominated peroxymonosulfate activation for organic pollutants degradation. *Chemosphere* **2021**, *285*, 131433.
(38) Chen, Z.; Bi, S.; Zhao, G.; Chen, Y.; Hu, Y. Enhanced degradation of triclosan by cobalt manganese spinel-type oxide activated peroxymonosulfate oxidation process via sulfate radicals and singlet oxygen: Mechanisms and intermediates identification. *Sci. Total Environ.* **2020**, *711*, 134715.
(39) Guo, S.; Wang, H.; Yang, W.; Fida, H.; You, L.; Zhou, K. Scalable synthesis of Ca-doped α-Fe2O3 with abundant oxygen vacancies for enhanced degradation of organic pollutants through peroxymonosulfate activation. *Appl. Catal., B* **2020**, *262*, 118250.
(40) Zhang, L.; Li, Y.; Guo, J.; Kan, Z.; Jia, Y. Catalytic ozonation mechanisms of Norfloxacin using Cu−CuFe2O4. *Environ. Res.* **2023**, *216*, 114521.
(41) Sun, Y.; Zhou, J.; Liu, D.; Li, X.; Liang, H. Enhanced catalytic performance of Cu-doped MnFe2O4 magnetic ferrites: Tetracycline hydrochloride attacked by superoxide radicals efficiently in a strong alkaline environment. *Chemosphere* **2022**, *297*, 134154.
(42) Wang, R.; An, H.; Zhang, H.; Zhang, X.; Feng, J.; Wei, T.; Ren, Y. High active radicals induced from peroxymonosulfate by mixed crystal types of CuFeO2 as catalysts in the water. *Appl. Surf. Sci.* **2019**, *484*, 1118−1127.
(43) Zhang, T.; Zhu, H.; Croué, J. P. Production of Sulfate Radical from Peroxymonosulfate Induced by a Magnetically Separable CuFe2O4 Spinel in Water: Efficiency, Stability, and Mechanism. *Environ. Sci. Technol.* **2013**, *47* (6), 2784−2791.
(44) Lewis, K. M.; Archer, R. D. pKa values of estrone, 17β-estradiol and 2-methoxyestrone. *Steroids* **1979**, *34* (5), 485−499.
(45) Aufartová, J.; Mahugo-Santana, C.; Sosa-Ferrera, Z.; Santana-Rodríguez, J. J.; Nováková, L.; Solich, P. Determination of steroid hormones in biological and environmental samples using green microextraction techniques: An overview. *Anal. Chim. Acta* **2011**, *704* (1−2), 33−46.
(46) Rani, S. K.; Easwaramoorthy, D.; Bilal, I. M.; Palanichamy, M. Studies on Mn(II)-catalyzed oxidation of α-amino acids by peroxomonosulphate in alkaline medium-deamination and decarboxylation: A kinetic approach. *Appl. Catal., A* **2009**, *369* (1−2), 1−7.
(47) Liu, Y.; He, X.; Fu, Y.; Dionysiou, D. D. Kinetics and mechanism investigation on the destruction of oxytetracycline by UV-254nm activation of persulfate. *J. Hazard. Mater.* **2016**, *305*, 229−239.
(48) Wu, Y.; Yang, Y.; Liu, Y.; Zhang, L.; Feng, L. Modelling study on the effects of chloride on the degradation of bezafibrate and carbamazepine in sulfate radical-based advanced oxidation processes: Conversion of reactive radicals. *Chem. Eng. J.* **2019**, *358*, 1332−1341.
(49) Wang, J.; Wang, S. Activation of persulfate (PS) and peroxymonosulfate (PMS) and application for the degradation of emerging contaminants. *Chem. Eng. J.* **2018**, *334*, 1502−1517.
(50) Qi, C.; Liu, X.; Ma, J.; Lin, C.; Li, X.; Zhang, H. Activation of peroxymonosulfate by base: Implications for the degradation of organic pollutants. *Chemosphere* **2016**, *151*, 280−288.
(51) Angkaew, A.; Sakulthaew, C.; Satapanajaru, T.; Poapolathep, A.; Chokejaroenrat, C. UV-activated persulfate oxidation of 17β-estradiol: Implications for discharge water remediation. *J. Environ. Chem. Eng.* **2019**, *7* (2), 102858.
(52) Jutarvutikul, K.; Sakulthaew, C.; Chokejaroenrat, C.; Pattanateeradetch, A.; Imman, S.; Suriyachai, N.; Satapanajaru, T.; Kreetachat, T. Practical use of response surface methodology for optimization of veterinary antibiotic removal using UV/H2O2 process. *Aquacult. Eng.* **2021**, *94*, 102174.
(53) Keen, O. S.; Love, N. G.; Linden, K. G. The role of effluent nitrate in trace organic chemical oxidation during UV disinfection. *Water Res.* **2012**, *46* (16), 5224−5234.
(54) Ghauch, A.; Tuqan, A. M. Oxidation of bisoprolol in heated persulfate/H2O systems: Kinetics and products. *Chem. Eng. J.* **2012**, *183*, 162−171.
(55) Deng, J.; Shao, Y.; Gao, N.; Xia, S.; Tan, C.; Zhou, S.; Hu, X. Degradation of the antiepileptic drug carbamazepine upon different UV-based advanced oxidation processes in water. *Chem. Eng. J.* **2013**, *222*, 150−158.
(56) Tan, C.; Gao, N.; Fu, D.; Deng, J.; Deng, L. Efficient degradation of paracetamol with nanoscaled magnetic CoFe2O4 and MnFe2O4 as a heterogeneous catalyst of peroxymonosulfate. *Sep. Purif. Technol.* **2017**, *175*, 47−57.
(57) Ji, Y.; Dong, C.; Kong, D.; Lu, J.; Zhou, Q. Heat-activated persulfate oxidation of atrazine: Implications for remediation of groundwater contaminated by herbicides. *Chem. Eng. J.* **2015**, *263*, 45−54.
(58) Barua, J. R. M.; Hussain, P.; Hazarika, R. A.; Kader, N. A.; Roy, N. K. Physicochemical Study of Livestock Farm Oriented Wastewater as a Source of Surface Water Pollution. *J. Anim. Res.* **2021**, *11*, 421−431.
(59) Zhang, T.; Chen, Y.; Wang, Y.; Le Roux, J.; Yang, Y.; Croué, J. P. Efficient Peroxydisulfate Activation Process Not Relying on Sulfate

https://doi.org/10.1021/acsomega.3c04333
ACS Omega 2023, 8, 36136−36151

Radical Generation for Water Pollutant Degradation. *Environ. Sci. Technol.* **2014**, *48* (10), 5868−5875.
(60) Shahzad, A.; Ali, J.; Ifthikar, J.; Aregay, G. G.; Zhu, J.; Chen, Z.; Chen, Z. Non-radical PMS activation by the nanohybrid material with periodic confinement of reduced graphene oxide (rGO) and Cu hydroxides. *J. Hazard. Mater.* **2020**, *392*, 122316.
(61) Zhu, Y.; Shao, Y.; Wei, M.; Yu, K.; Zhang, Y.; Huang, J.; Yin, X. Degradation of 17β-estradiol by UV/persulfate in different water samples. *J. Water Health* **2021**, *19* (5), 796−807.
(62) Hu, J.; Cheng, S.; Aizawa, T.; Terao, Y.; Kunikane, S. Products of Aqueous Chlorination of 17β-Estradiol and Their Estrogenic Activities. *Environ. Sci. Technol.* **2003**, *37* (24), 5665−5670.
(63) Ohko, Y.; Iuchi, K.-i.; Niwa, C.; Tatsuma, T.; Nakashima, T.; Iguchi, T.; Kubota, Y.; Fujishima, A. 17β-Estradiol Degradation by TiO2 Photocatalysis as a Means of Reducing Estrogenic Activity. *Environ. Sci. Technol.* **2002**, *36* (19), 4175−4181.
(64) Sakulthaew, C.; Comfort, S.; Chokejaroenrat, C.; Harris, C.; Li, X. A combined chemical and biological approach to transforming and mineralizing PAHs in runoff water. *Chemosphere* **2014**, *117*, 1−9.
(65) Fragkaki, A. G.; Angelis, Y. S.; Koupparis, M.; Tsantili-Kakoulidou, A.; Kokotos, G.; Georgakopoulos, C. Structural characteristics of anabolic androgenic steroids contributing to binding to the androgen receptor and to their anabolic and androgenic activities. *Steroids* **2009**, *74* (2), 172−197.
(66) Erdal, S.; Dumlupinar, R. Progesterone and β-Estradiol Stimulate Seed Germination in Chickpea by Causing Important Changes in Biochemical Parameters. *Z. Naturforsch. C* **2010**, *65* (3−4), 239−244.
(67) Shore, L. S.; Kapulnik, Y.; Ben-Dor, B.; Fridman, Y.; Wininger, S.; Shemesh, M. Effects of estrone and 17 β-estradiol on vegetative growth of Medicago sativa. *Physiol. Plant.* **1992**, *84* (2), 217−222.
(68) Bowlin, K. M. Effect of β-estradiol on germination and growth in Zea Mays L. M.Sc. Thesis, Department of Natural Sciences in Northwest Missouri State University, Maryville, USA, 2014. https://www.nwmissouri.edu/library/theses/2014/BowlinKelseyM.pdf.
(69) Zhang, Y.; Nie, S.; Nie, M.; Yan, C.; Qiu, L.; Wu, L.; Ding, M. Remediation of sulfathiazole contaminated soil by peroxymonosulfate: Performance, mechanism and phytotoxicity. *Sci. Total Environ.* **2022**, *830*, 154839.
(70) Xu, X.; Du, X.; Wang, F.; Sha, J.; Chen, Q.; Tian, G.; Zhu, Z.; Ge, S.; Jiang, Y. Effects of Potassium Levels on Plant Growth, Accumulation and Distribution of Carbon, and Nitrate Metabolism in Apple Dwarf Rootstock Seedlings. *Front. Plant Sci.* **2020**, *11*, 904.
(71) Jordan, V. C. The 38th David A. Karnofsky lecture: the paradoxical actions of estrogen in breast cancer−survival or death? *J. Clin. Oncol.* **2008**, *26* (18), 3073−3082.
(72) Hassan, M. H.; Salama, S. A.; Zhang, D.; Arafa, H. M.; Hamada, F. M.; Fouad, H.; Walker, C. C.; Al-Hendy, A. Gene therapy targeting leiomyoma: adenovirus-mediated delivery of dominant-negative estrogen receptor gene shrinks uterine tumors in Eker rat model. *Fertil. Steril.* **2010**, *93* (1), 239−250.

https://doi.org/10.1021/acsomega.3c04333
ACS Omega 2023, 8, 36136−36151